NAVAL POSTGRADUATE SCHOOL
Monterey, California

THESIS

PRECISION AIR DATA SUPPORT FOR CHEM/BIO ATTACK RESPONSE

by

Kwang Liang Tan

March 2003

Thesis Advisor: Richard M. Howard
Second Reader: Vladimir N. Dobrokhodov

Approved for public release; distribution is unlimited

THIS PAGE INTENTIONALLY LEFT BLANK

REPORT DOCUMENTATION PAGE		*Form Approved OMB No. 0704-0188*

Public reporting burden for this collection of information is estimated to average 1 hour per response, including the time for reviewing instruction, searching existing data sources, gathering and maintaining the data needed, and completing and reviewing the collection of information. Send comments regarding this burden estimate or any other aspect of this collection of information, including suggestions for reducing this burden, to Washington headquarters Services, Directorate for Information Operations and Reports, 1215 Jefferson Davis Highway, Suite 1204, Arlington, VA 22202-4302, and to the Office of Management and Budget, Paperwork Reduction Project (0704-0188) Washington DC 20503.

1. AGENCY USE ONLY *(Leave blank)*	2. REPORT DATE March 2003	3. REPORT TYPE AND DATES COVERED Master's Thesis	
4. TITLE AND SUBTITLE Precision Air Data Support for Chem/Bio Attack Response		5. FUNDING NUMBERS	
6. AUTHOR (S) Kwang Liang Tan			
7. PERFORMING ORGANIZATION NAME(S) AND ADDRESS(ES) Naval Postgraduate School Monterey, CA 93943-5000		8. PERFORMING ORGANIZATION REPORT NUMBER	
9. SPONSORING / MONITORING AGENCY NAME(S) AND ADDRESS(ES) NA		10. SPONSORING/MONITORING AGENCY REPORT NUMBER	
11. SUPPLEMENTARY NOTES The views expressed in this thesis are those of the author and do not reflect the official policy or position of the U.S. Department of Defense or the U.S. Government.			
12a. DISTRIBUTION / AVAILABILITY STATEMENT Approved for public release; distribution is unlimited		12b. DISTRIBUTION CODE	

13. ABSTRACT *(maximum 200 words)*

The defense response against chemical and biological (Chem/bio) weapons has gained a renewed focus in light of the 11 Sept 2001 terrorist attack. A successful response to a Chem/bio attack would involve measuring and predicting the dispersion of a toxic cloud in the atmosphere. The NPS Aeronautics and Astronautics Department is working together with the Meteorology Department on a technique to make toxic cloud measurements using an Unmanned Air Vehicle (UAV). In support of this mission, the UAV will require precise and accurate air data (airspeed, angle of attack ["alpha"], and sideslip angle ["beta"]) so that wind data extraction can be carried out from air and inertial data for use in plume dispersion modeling. The efforts in this thesis concentrate on the air data system to produce precise and accurate air data for the support of the Chem/bio response UAV flights. The primary concerns are the choice and design of the air data system; the calibration of the system using the flow fields from computer simulation; and the processing of air data. The air data extracted will be used for wind determination so that the movement of the Chem/bio dispersed agent in the atmosphere can be predicted.

14. SUBJECT TERMS Unmanned Aerial Vehicles, UAV, Air data, Chem/Bio			15. NUMBER OF PAGES 122
			16. PRICE CODE
17. SECURITY CLASSIFICATION OF REPORT Unclassified	18. SECURITY CLASSIFICATION OF THIS PAGE Unclassified	19. SECURITY CLASSIFICATION OF ABSTRACT Unclassified	20. LIMITATION OF ABSTRACT UL

NSN 7540-01-280-5500

Standard Form 298 (Rev. 2-89)
Prescribed by ANSI Std. 239-18

THIS PAGE INTENTIONALLY LEFT BLANK

PRECISION AIR DATA SUPPORT FOR CHEM/BIO ATTACK RESPONSE

Kwang Liang Tan
Captain, Republic of Singapore Air Force
B.Eng.(Mechanical), Nanyang Technological University, 1997

Submitted in partial fulfillment of the
requirements for the degree of

MASTER OF SCIENCE IN AERONAUTICAL ENGINEERING

from the

**NAVAL POSTGRADUATE SCHOOL
March 2003**

Author: Kwang Liang Tan

Approved by: Richard M. Howard
                Thesis Advisor

                Vladimir N. Dobrokhodov
                Second Reader

                Max F. Platzer
                Chairman
                Department of Aeronautics and Astronautics

THIS PAGE INTENTIONALLY LEFT BLANK

ABSTRACT

The defense response against chemical and biological (Chem/bio) weapons has gained a renewed focus in light of the 11 Sept 2001 terrorist attack. A successful response to a Chem/bio attack would involve measuring and predicting the dispersion of a toxic cloud in the atmosphere. The NPS Aeronautics and Astronautics Department is working together with the Meteorology Department on a technique to make toxic cloud measurements using an Unmanned Air Vehicle (UAV). In support of this mission, the UAV will require precise and accurate air data (airspeed, angle of attack ["alpha"], and sideslip angle ["beta"]) so that wind data extraction can be carried out from air and inertial data for use in plume dispersion modeling. The efforts in this thesis concentrate on the air data system to produce precise and accurate air data for the support of the Chem/bio response UAV flights. The primary concerns are the choice and design of the air data system; the calibration of the system using the flow fields from computer simulation; and the processing of air data. The air data extracted will be used for wind determination so that the movement of the Chem/bio dispersed agent in the atmosphere can be predicted.

THIS PAGE INTENTIONALLY LEFT BLANK

TABLE OF CONTENTS

LIST OF FIGURES

LIST OF TABLES

THIS PAGE INTENTIONALLY LEFT BLANK

NOMENCLATURE

p_t	total pressure
p	static pressure
q_c	impact pressure
q	dynamic pressure
ρ	density of air ρ
α	angle of attack
β	sideslip angle
u, V_x	x-component of velocity vector
v, V_y	y-component of velocity vector
w, V_z	z-component of velocity vector
V	velocity vector
α_f	flank angle of attack
ΔV_{pc}	velocity position error
$\Delta \alpha_{pc}$	α position error
$\Delta \beta_{pc}$	β position error
ΔC_{p-pc}	position error pressure coefficient
ΔH_{pc}	altitude position correction
σ_{std}	standard day density ratio
g_o	gravitational constant
$K\alpha$	upwash factor on α
$K\beta$	upwash factor on β
p	roll rate

q	pitch rate
r	yaw rate
^iV_w	wind vector in the inertial coordinate system
$^iV_{b,i}$	FROG velocity in inertial coordinate system
^i_wR	rotation transformation matrix from wind to inertial coordinate system
$V_{b,w}$	FROG velocity in the wind coordinate system
λ	lag constant

ACKNOWLEDGEMENTS

THIS PAGE INTENTIONALLY LEFT BLANK

DISCLAIMER

The mention of commercial products in this thesis does not imply endorsement by the United States of America Government.

I   INTRODUCTION

A.   BACKGROUND

Chemical and biological (Chem/Bio) weapons have posed a defense response security concern for some time and have, in light of the 11 September 2001 terrorist attack, gained a renewed focus. The dispersion of a toxic cloud is important to measure and predict in order to successfully respond to attacks by such weapons. The work in this thesis supports the Chem/Bio response project which is a joint project between the NPS Aeronautics and Astronautics Department and Meteorology Department to demonstrate and validate a method for the synthesis of measurements and predictions to aid in the response to an attack by chemical and biological weapons. The use of a UAV to make in situ measurements of particulates as well as air and inertial data for winds extraction is a unique contribution to the area of homeland security.

One of the key features of the Chem/Bio response project will be the movement prediction of the Chem/Bio plume with a UAV equipped with a proper sensor suite. In support of this mission, this thesis research concentrates on the air data system to produce precise and accurate air data for the support of the Chem/bio response UAV flights. The primary concerns are the choice and design of the air data system, the calibration of the air data system using the flow field from computer simulation and the processing of air data so that data extraction for wind determination can be carried out.

B.   OBJECTIVES

This thesis seeks to implement an air data system using standard sensors on the NPS FROG UAV (refer to next section or [4] for more details on the FROG UAV). With the air data system implemented, test flights are to be carried out so that air data can be acquired, processed and analyzed. Wind data can then be extracted for support of the Chem/Bio attack response UAV project.

In addition, this thesis explores better quality and precision air data sensors for use on the FROG. This is to improve the quality of air data so as to enhance the wind data extraction which is highly dependent on the quality of air data acquired.

Details of both of these objectives will be covered in the subsequent chapters.

II AIR DATA SYSTEM

A. THE FOG-R UAV (THE FROG)

The NPS's UAV, the FROG, as shown in Figure II.1, has been the test bed for advanced control and airborne sensor projects at NPS. It is manufactured by BAI Aerosystems as the BAI-TERN (Tactically Expendable Remote Navigator) and derives from the FOG-R variant of the BAI-TERN used by the US Army, hence the name 'FROG'.

It is a small high wing monoplane with conventional elevator, rudder, ailerons and flaps, and uses servo-motors designed for radio-controlled airplanes to drive the control surfaces. It has a pod and boom fuselage with high mounted wing, sweptback fin and rudder and low set tailplane. The wings are fitted with flaps and the engine is mounted above the wing center section. The landing gear is that of a fixed tricycle type. The launch and recovery are that of conventional wheeled take-off and landing respectively. More details on its physical characteristics and engine are documented in Appendix A.

Figure II.1 NPS FROG UAV
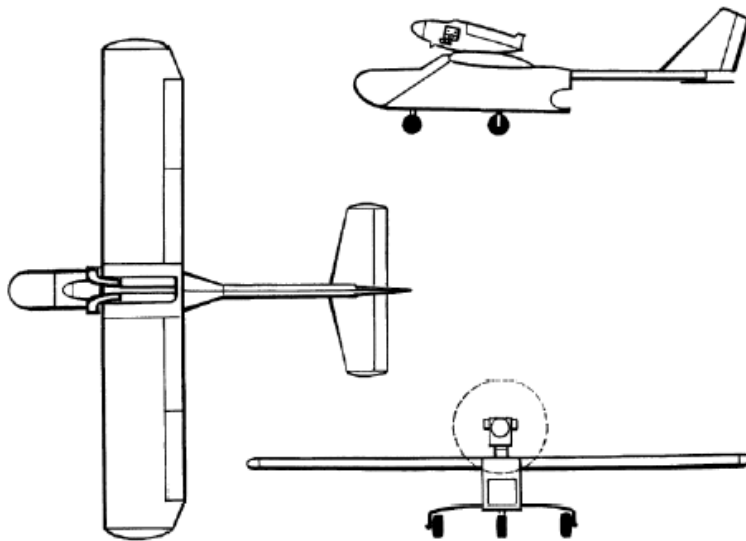
Figure II.2 FROG UAV 3 View Drawing

B.   AIRSPEED SENSOR

Two basic pressures, static and total pressure, are used for measurement of airspeed. The static pressure is the atmospheric pressure at the flight level of the

aircraft, while the total pressure is the sum of the static and the impact pressure, which is the pressure developed by the forward speed of the aircraft. The relation of the three pressures can thus be expressed by the following equation:

$$p_t = p + q_c \qquad\qquad (1)$$

Where p_t is the total pressure, p is the static pressure, and q_c the impact pressure.

In incompressible flow, the pressure developed by the forward motion of a body is called the dynamic pressure q, which is related to the true airspeed V by the equation:

$$q = \frac{1}{2}\rho V^2 \qquad\qquad (2)$$

Where ρ is the density of the air and V is the speed of the aircraft relative to the air.

For compressible flow, the measured impact pressure q_c is higher than the dynamic pressure and the effects of compressibility must be taken into account. Since the FROG operates in the low subsonic range, compressibility effects are ignored.

The airspeed of the FROG is computed based on dynamic pressure measurement using a pitot-static probe (mounted at the wingtip) and pressure transducers. The dynamic pressure is 'fed' into a pressure transducer that in turn converts it to analog voltage signal. With proper calibration and

application of Equation (2), the airspeed of the UAV can be computed. Subsequent sections will explain the rationale for mounting the probe at the wing tip rather than at the nose or any other locations on the FROG.

The pitot-static probe is a straight conventional type. The total length of the probe is 26 inches long and the four static pressure sensing ports are located 1.125 inches aft of the total pressure port; 6 diameters (of the probe) aft. Figure II.3 shows the pitot-static probe mounted on the aircraft and Figure II.4 shows the actual probe.

The pressure transducer used is a 0-4 inches H_2O differential pressure transducer. It takes in a single power supply between 7.5 to 24 volts and gives an output signal of 0 to 5 volts. It is precision temperature compensated, calibrated and has an operating temperature range of −10 $^{\circ}C$ to 70 $^{\circ}C$. It has a proof pressure of 10 inches H_2O and hence if the input differential pressure exceeds the proof pressure, the sensing element of the transducer will be damaged. Figure II.5 shows the actual pressure transducer.

Figure II.3 Pitot-static probe mounted on FROG

Total pressure
sensing port

Static pressure
sensing ports
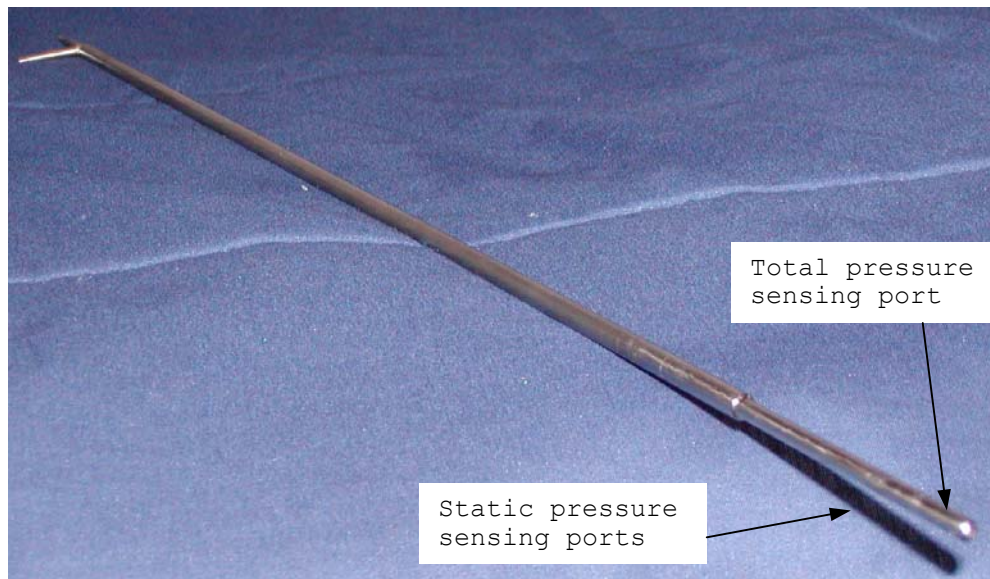
Figure II.4 Pitot-static probe layout
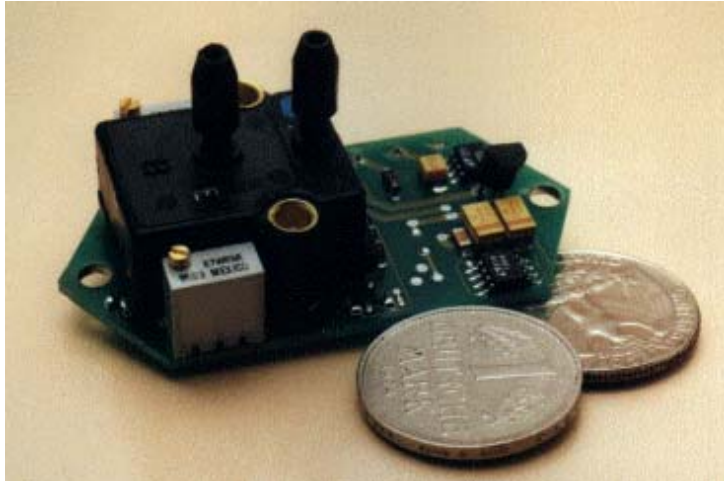
Figure II.5 Pressure transducer for airspeed measurement

C.   **ANGLE OF ATTACK AND SIDESLIP ANGLE SENSOR**

Angle of attack (alpha, α) is defined as the angle between the relative wind in the plane of symmetry and the longitudinal axis of the aircraft. Sideslip (beta, β) angle is defined as the angle between the wind vector and the plane of symmetry. Figure II.6 illustrate the definitions. Wind vanes mounted on potentiometers (pots) are used to measure α and β. Note that the β vane actually measures 'flank angle of attack' but since α is small, true β can be approximated by 'flank angle of attack'.

8

$$\alpha = \tan^{-1} \frac{w}{u} \qquad \beta = \sin^{-1} \frac{v}{V}$$

$$\alpha_f = \tan^{-1} \frac{v}{u}$$
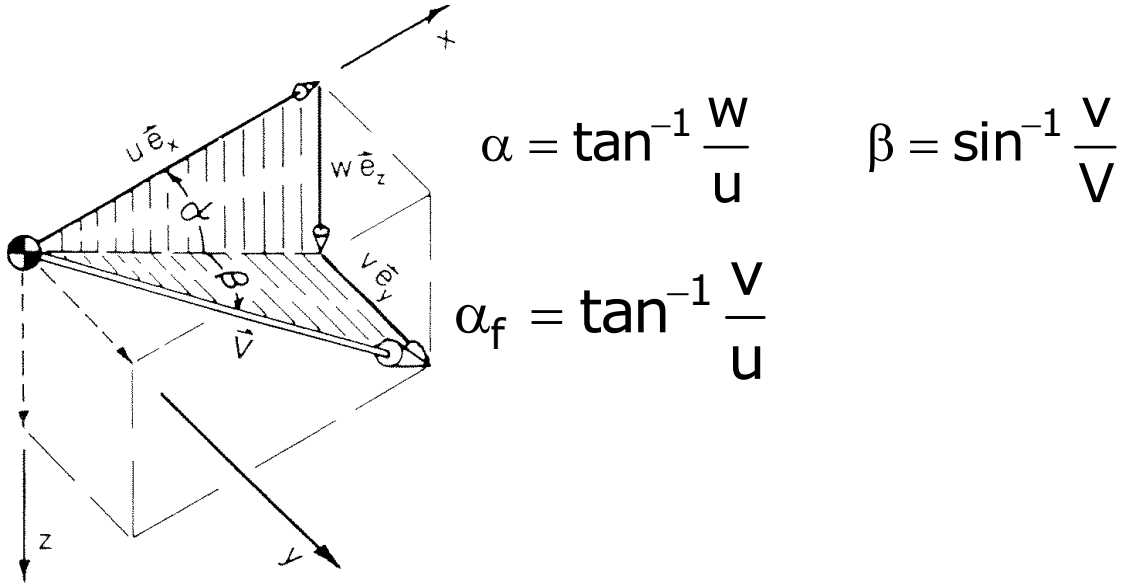
Figure II.6 α and β definitions (From [8])

The vane-pots assembly is mounted on a probe that is similar to the pitot-static probe at the wing tip. The wind vanes are attached to the shaft of the pots. As the UAV pitches and/or yaws, the vanes rotate and that causes the shaft to rotate. The rotation of the shafts changes the resistance of the pots and since a voltage is applied across the pots from the FROG's power supply, an analog output voltage signal is produced. With proper calibration, the α-β of the UAV will then be obtained.

The pot used is a low torque pot that has a maximum running torque of 0.05 ounce-inch. It has a resistance of 10 kΩ ± 5% with a linearity of ± 1%. The maximum power rating is 2 watts at 40 $^{\circ}$C. The shaft is made from stainless steel that is non-magnetic and non-reactive. It has a rotational life of 500,000 shaft revolutions and a load life of 900 hours. It is to be operated in the temperature

range of –55 °C to 125 °C. Figure II.7 shows the actual $\alpha - \beta$ vanes mounted on the pots. The data specifications for the pots can be found in Appendix B.

The wind vanes that will be mounted on the pots are made of light weight graphite and the vanes are mass balanced to eliminate biasing errors.
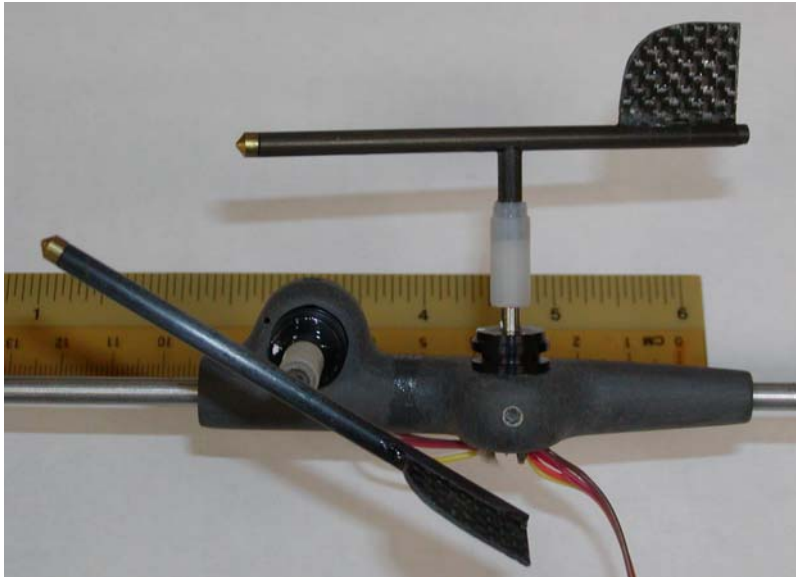
Figure II.7 $\alpha - \beta$ vanes mounted on the pots

D.   DATA ACQUISITION PACKAGE

Apart from the sensors described in the previous sections, the remaining air data system components include a processor with 12-bit analog to digital converter, a spread-spectrum radio modem (refer to Figure II.8) and a ground station computer which make up the data acquisition package. The processor is a data logger operating with either TXBASIC or C (programming language). It consists of a PIC microprocessor, a +5 volts switching power supply,

and a +3 volts low power supply for energy conservation. There are two serial RS232 ports and eight TP lines available that can be programmed as digital serial input, output lines or other functions. The communication link between the UAV and the ground station computer is implemented with a wireless modem. The modem uses frequency hopping spread spectrum technology and has a power output of 1/3 watts. It is capable of communicating over a line of sight range of up to 20 miles, and supports data transmission at baud rates from 1200 bps to 115.2 kbps. The ground station computer basically does the real time download and storage of the air data transmitted down from the FROG via the modem.

Figure II.8 Modems; both the aircraft and ground station computer has one unit each

E. INTEGRATION OF AIR DATA SYSTEM

The schematic of the air data system is as shown in Figure II.9. For clarity, other sensors, for example, rate gyros, humidity sensors, etc. are not included in Figure II.9. The air data system is such that the data acquired is post processed rather than real time processed. (It can be real time processed and real time processing of air data is researched in [9]). The pitot-static probe allows dynamic pressure to be measured via pressure tubing by the pressure transducer. The transducer basically converts the pressure pulses into an analog signal and the signal is transmitted to the processor. As for α-β measurement, the pots generate an analog signal and through shielded wires, the signal goes into the processor. The processor basically converts both analog signals to digital signals. The digital signals then go into the modem onboard the aircraft and are transmitted to the ground station computer. A MATLAB® script file is used as the software package to acquire the data so that it can be post processed either with MATLAB® or any spreadsheet program.
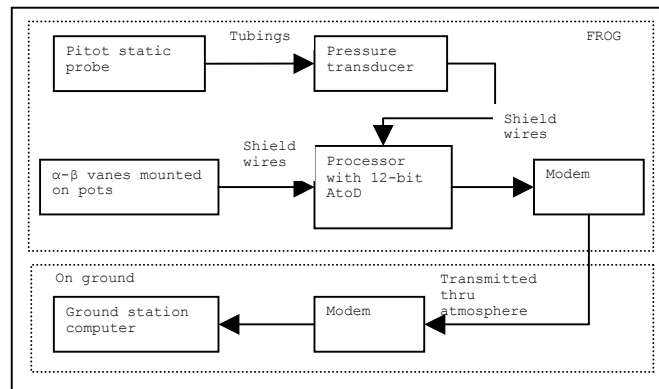
Figure II.9 Schematic of air data system

12

F. PRECISION OF AIR DATA MEASUREMENT

1. Airspeed Precision and Accuracy

a.   *Total Pressure Measurement*

The equation of airspeed is based on the measurement of the impact pressure and it is derived from measured values of total and static pressures. The static pressure at successive points along lines of airflow past a body can vary widely, whereas the total pressure along these lines of flow remains constant. For this reason, the measurement of total pressure is much less difficult than the measurement of static pressure.

When aligned with the flow, almost any open ended probe registers total pressure correctly provided that the tube is located away from any boundary layer, wake, propeller slip stream, or engine exhaust. As far as the FROG is concerned, the pitot-static probe is mounted at the wingtip which has minimal effect from any boundary layer, wake, propeller slip stream, or engine exhaust.

b.   *Static Pressure Measurement*

The flow of the air over a body creates a pressure field in which the static pressure varies from point to point, while the total pressure at all points remains the same. For this reason, the measurement of static pressure is much more complicated and therefore, the problem of designing a static pressure measuring system is primarily one of finding a location where the static

pressure error varies by the least amount throughout the operating range of the aircraft.

Figure II.10 from [1] shows four typical types of static pressure measuring installations (static pressure tubes ahead of the fuselage nose, wing tip, vertical fin and fuselage vent on the side of the fuselage).
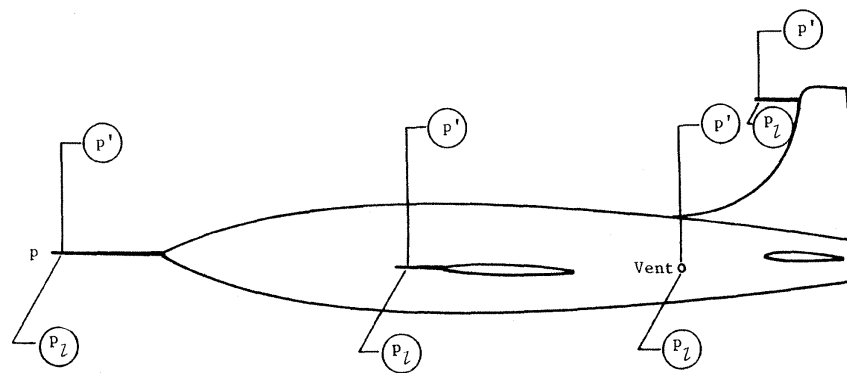
p   free-stream static pressure

p_l local static pressure

p   pressure sensed by static-pressure tube or fuselage vent

Δp position error, p'- p

Figure II.10 Typical installations for measurement of
static pressure on an aircraft (From [1])

(1)   Fuselage-Nose Installation. For a given position of static pressure orifices ahead of the nose of a fuselage, the static pressure error depends on the shape of the fuselage nose and the maximum diameter of the fuselage. Figure II.11 shows the variation of the static pressure error with the blocking effect (reference to Figure II.11, x/D). As far as the FROG is concerned, if the static pressure measurement is made with a fuselage-nose installation, the error will be 8% as the blocking

14

effect is about 0.75 since x is about 20 inches and D is about 26 inches. Using a longer probe does reduces the error; however, one may encounter vibration problems.
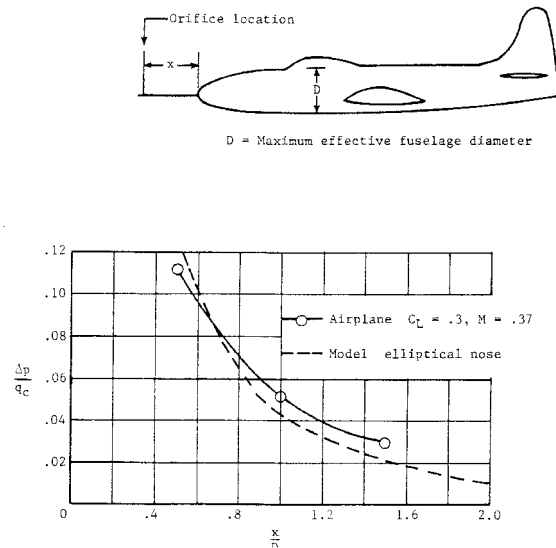
Figure II.11 Static pressure error variation with blocking effect (From [1])

(2)   Wing-tip installation. For a given position of static pressure orifices ahead of the wing, the magnitude and variation of the error depend on the shape of the airfoil section, the maximum thickness of the airfoil and the spanwise location of the boom. The magnitude of the errors ahead of a wing tip is shown in Figure II.12. The figure shows that the error is highest at the position closet to the wing and it decrease rapidly to a value of about 1% q_c at an orifice location of $x/t = 10$, beyond which further reduction in the error is minimal. For the FROG, having the wing-tip installation means an error of about 1% since $x/t = 8$.

15

Orifice
location

t = Maximum wing thickness
at spanwise location of boom

x

Tube A

.08

.06

$\frac{\Delta p}{q_c}$ .04

.02

Six orifice positions x/t
on above airplane
at C_L = .2 and M = .30
1-chord booms on nine other
airplanes at C_L = .2

12   16   20

$\frac{x}{t}$
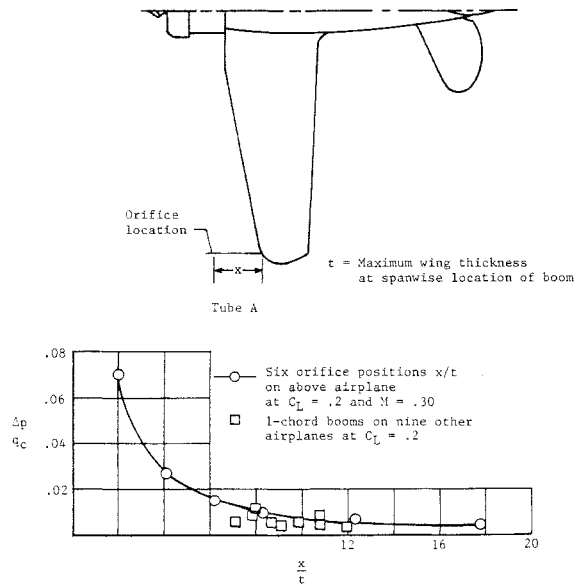
Figure II.12 Static pressure error at various positions
ahead of wing tips (From [1])

        (3)   Vertical-fin   installation.   The
factors that affect the measurement of the static pressure
ahead of a vertical fin are similar to those for wing-tip
installations. As far as the FROG is concerned, using a
vertical-fin installation to measure static pressure
presents some degree of mechanical complexity due to the
aircraft layout. Hence this option was not considered.

        (4)   Fuselage   vent   installation.   The
fuselage is in a general way a 'static-pressure tube'. When
the fuselage is aligned with the air flow, the pressure at
a vent is determined by its location along the body, and
when the fuselage is inclined to the flow, the pressure is
dependent on the radial position of the orifice around the
body. Similar to the vertical fin installation, the
fuselage vent installation is not considered for the FOG-R
due to the complex nature.

16

Considering the fuselage-nose and wing tip installations, the latter was selected due to the very low associated errors.

c. *Pressure Lag and Leak*

The pressure at a sensor can be different from the pressure at the pressure source because of a time lag in the transmission of pressures. The pressure at the instrument can also differ from that at the pressure source when there is a leak in the pressure system. For both cases, the sensor indications will be in error by an amount corresponding to the pressure drop in the system.

(1) Pressure lag. When the pressure at the pressure source is changing rapidly, as in the case of high-speed dives or climbs, the pressure at the instruments lags behind the pressure at the source because of (1) the time for the pressure change to propagate along the tubing (acoustic lag) and (2) the pressure drop associated with the flow through the tubing (pressure lag).

From [1], errors associated with acoustic lag are estimated to be negligible since the pressure tubing used in the FROG is relatively short (80 inches of tubing used). As far as pressure lag is concerned, calculations can be carried out to find the lag constant and rate of pressure change and pressure drop. However, [1] concluded that for relatively simple pressure systems with few bends and tees in the tubing, which the FROG certainly has, pressure lag is not an issue.

(2) Pressure leak. The pressure at the instrument can be different from that at the pressure source if there is a leak in the system and if the pressure outside the system is different from that inside. The magnitude of the pressure error due to a leak depends on the size of the leak and the pressure drop across the leak.

The errors in airspeed that result from a leak of a given size and a given pressure differential across the leak can be determined from the leak rate and lag constant. As far as the FROG is concerned, it is valid to assume that there are no or minimal pressure leaks since very little pressure tubing connections are present and numerous checks have been carried out.

2. α and β Precision and Accuracy

Due to the flow field created by the aircraft, the flow angle at any given location in the vicinity of the aircraft will generally differ from the true α and/or β. As the flow field around each different aircraft configuration is unique, the α and/or β errors (i.e. the difference between local and true angles) at a given location with respect to the aircraft will vary from one aircraft to another and more importantly, from one trim flight condition to another. For the FROG, the position errors will be estimated via numerical computation to be presented in subsequent chapters and sections. The three sensor positions which have been proven successful and which have been used to the greatest extent are positions

ahead of the fuselage nose, ahead of the wing tip, and on the forebody of the fuselage.

From [2], it has been concluded that for operation throughout the subsonic, transonic and supersonic speed range, a position ahead of the fuselage will provide the best installation. For the FROG, having the fuselage nose installation for the FROG does present an operational problem since the nose compartment is the primary payload compartment with many electronic components in it, requiring frequent access. The wing-tip installation was finally chosen due to ease of fabrication, implementation and operation. For α and β measurement, the wing tip installation does present a greater error compared to the fuselage nose installation due to the lift characteristic of the wing; however, that can be corrected (as presented in subsequent sections).

G.   CALIBRATION OF SENSORS

Calibration of the sensors is necessary to correlate the results in desired units with the output digital signal from the processor in the data acquisition package. The calibration of the pressure transducer was carried out and the results are plotted in Figure II.13. For this transducer, the output voltage was found to vary linearly with the delta pressure as designed by the manufacturer. A first order curve fitting was carried out and yielded the following equation:

Delta pressure [pascal] = 0.0315 x (output voltage [volts]) - 1.7781   (3)

19
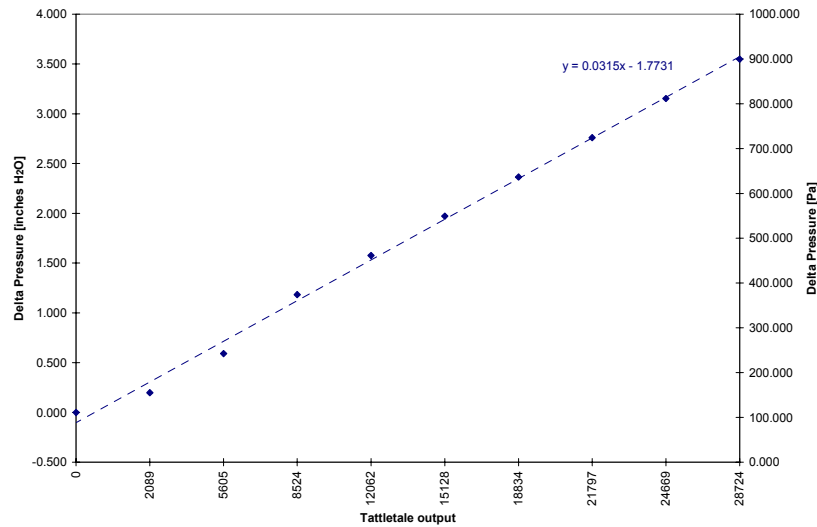
Figure II.13 Calibration curve for pressure transducer

Equation (3) allows the processing of the airspeed data acquired to be carried out. The pressure range of the transducer in terms of inches of water is also shown in Figure II.13 for comparison purposes. Equivalent indicated airspeed will be obtained from Equation (3) and this will be shown in Chapter III.

Similar to the pressure transducer, the $\alpha - \beta$ pots were calibrated and the results of the calibration of both of the pots are presented Figure II.14.

Alpha Beta POT Calibration (Done on aircraft)
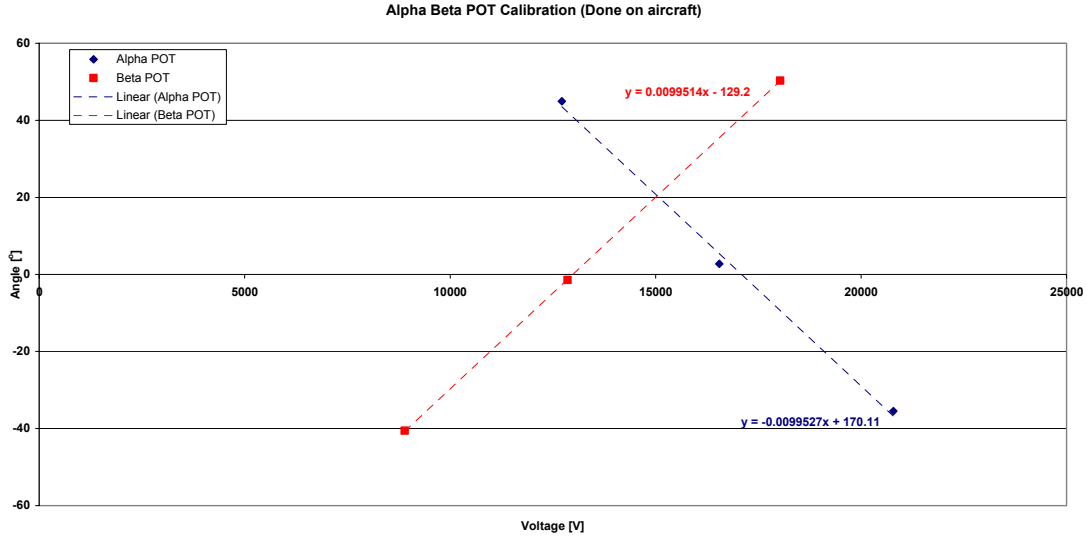
Figure II.14 Calibration curve for $\alpha - \beta$ pots; positive β is defined as 'wind in right ear'

From Figure II.14, both the $\alpha - \beta$ pots output voltages were found to vary linearly with the relative angle. The useful range of the pots will be ±20° since the FROG is not expected to fly at any α or β greater than 20° or lesser than -20°. Note that the input reference voltage supplied to the pots was 4 volts. A first order curve fitting was carried out and yielded the following equations:

α [°] = -0.0099527 x (Output voltage [Volts]) + 170.11

(4)

β [°] = 0.0099514 x (Output voltage [Volts]) – 129.2

(5)

Since the pressure transducer used is a 0-4 inches H_2O differential type with an output analog signal of 0-5

volts, this translated to a full range of 0-40.4 meters per second of equivalent airspeed. As the processor in the data acquisition package has a 12-bit analog to digital converter with input voltage of 0-4.096 volts, the resolution of the airspeed sensor is $\dfrac{40.4}{\dfrac{5}{4.096}2^{12}} \approx 0.008$ meters per second. Since the useful range of the $\alpha - \beta$ pots (40°) does not span an output analog signal of 0-5 volts but rather 2.76-3.23 volts, the resolution of the $\alpha - \beta$ sensor is $\dfrac{40.0}{(\dfrac{3.23}{4.096} - \dfrac{2.76}{4.096})2^{12}} \approx 0.09^{\circ}$. More details on resolution will be covered in Chapter VI.

III AIR DATA PROCESSING

A. FLIGHT TEST PROFILE AND PROCESSING OF AIR DATA

The FROG was flown at Camp Roberts on 9 Oct 2002 to check out the air data system as well as to acquire air data. The test flight was conducted at the McMillan Airfield at Camp Roberts, California. The flight profile was straight and level passes on the runway heading with a turn at each end at an approximate flight level of 50 feet AGL. Figure III.1 shows the flight profile of the test flight obtained with the GPS unit onboard the FROG and an aerial photo of the airfield. The flight profile is in GPS coordinates (longitudinal minutes versus lateral minutes).
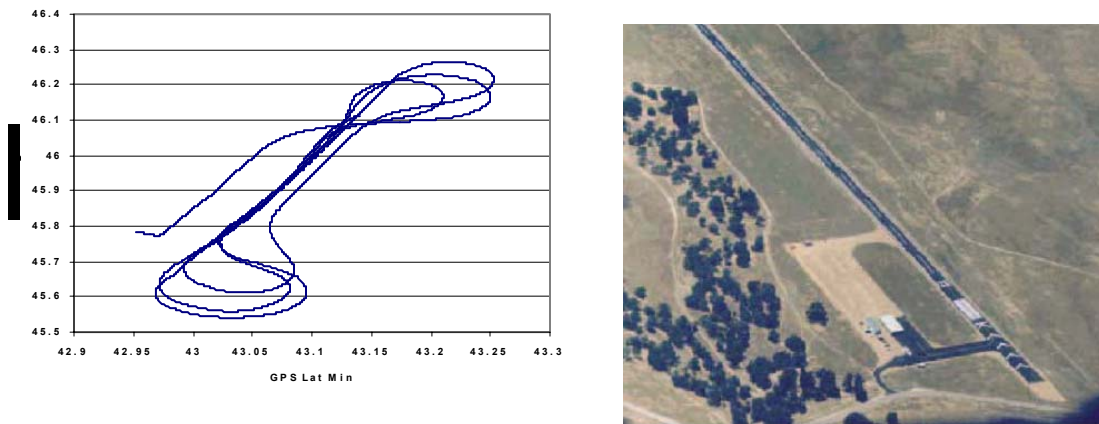
Figure III.1 Flight profile of FROG during test flight (left) and McMillan Airfield (right)

The air data acquired from the test flight was post processed. Post processing of the air data involved filtering, re-sampling, calibrating and making corrections. The next few sections explain the details of the filtering, re-sampling, calibrating and correction process. The air

data post processed will be analyzed in Chapter IV; the air data was correlated with the flight profile flown to check the sanity of the air data.

B.   FILTERING

It is vital to filter the data signals to remove unwanted noise. This is done via power spectrum density (PSD) analysis and software filtering using the Signal Processing Toolbox (SPTool$^{®}$) in MATLAB$^{®}$. The airspeed data was sampled at a frequency of 20 hertz while the $\alpha - \beta$ data was sampled at 40 hertz. Figures III.2 through III.4 show the PSD plots of the three signals. It is obvious from the plots that the air data of interest is of low frequency; note the peaks of the PSD plots at very low frequencies. The frequency of noise was in the range of 1.5 hertz and above.
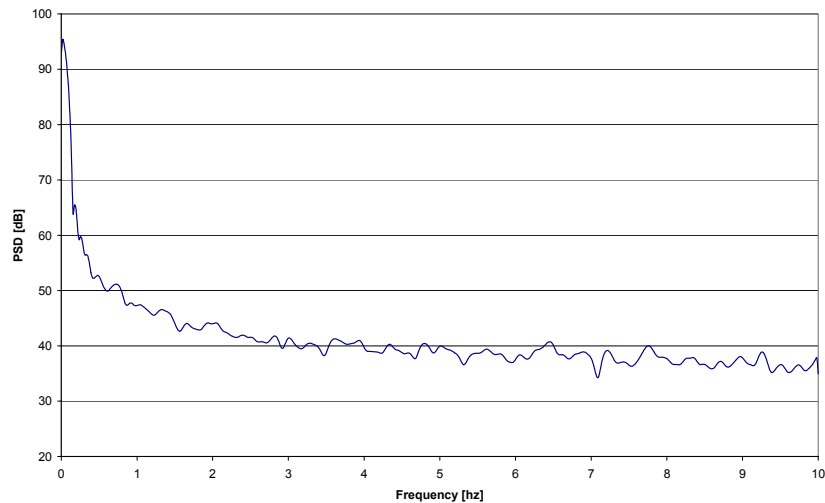
Figure III.2 PSD plot of unprocessed airspeed data
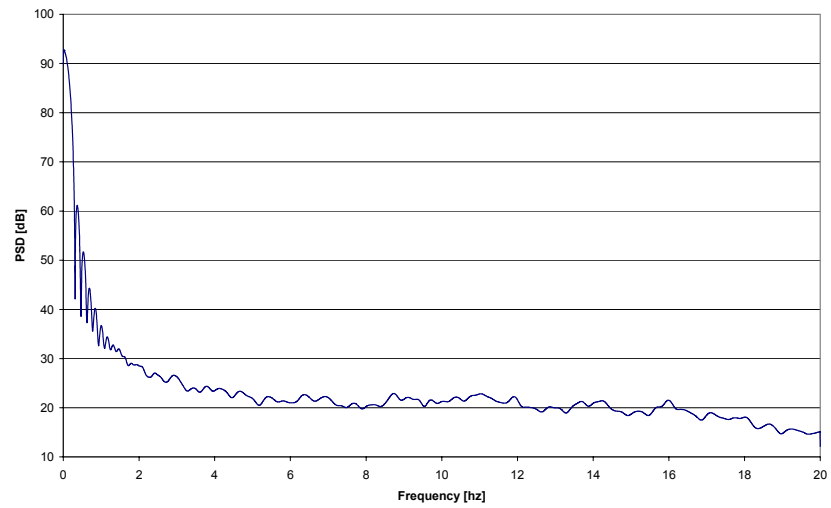
Figure III.3 PSD plot of unprocessed α data
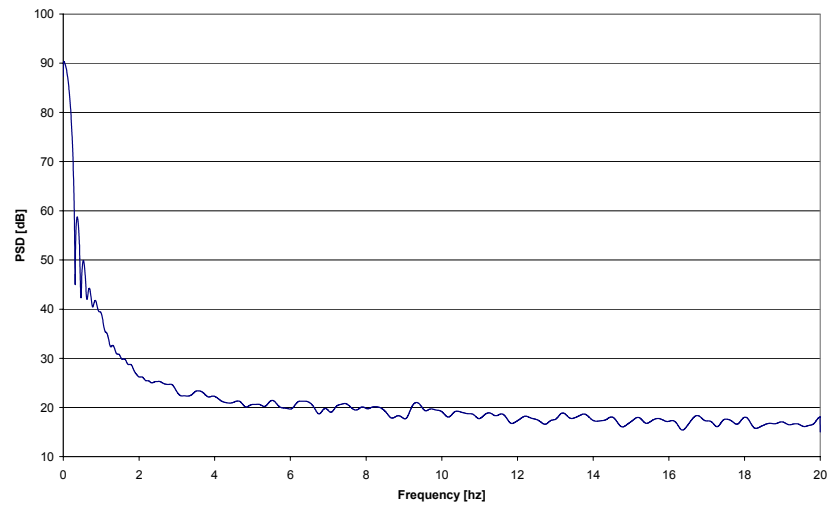
Figure III.4 PSD plot of unprocessed β data

Using the MATLAB® Signal Processing Toolbox, low-pass filters were designed (with the auto-design feature) using the Chebyshev type II IIR algorithm. For the airspeed data low-pass filter, the cut-off frequency is 0.5 hertz while

25

the cut-off frequency for the $\alpha - \beta$ data low-pass filter is 2 hertz. The cut-off frequencies were auto-generated by the auto-design feature and manually checked for sanity before the filters were applied. Figures III.5 through III.10 show the signals before and after filtering.
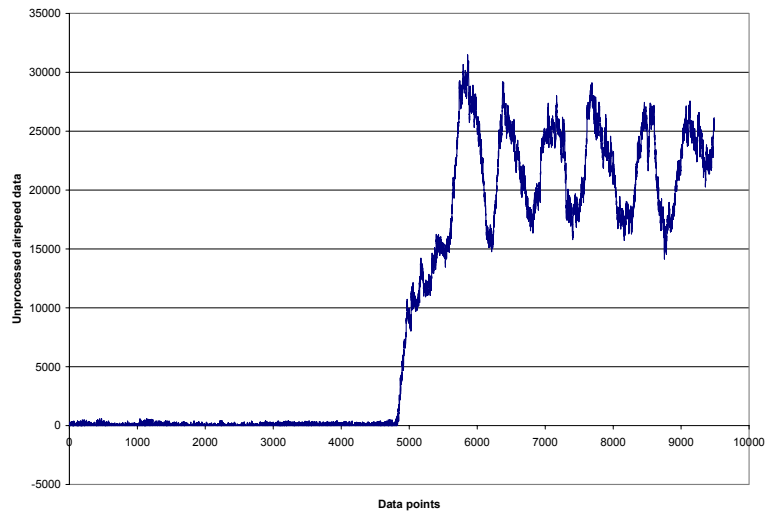
Figure III.5 Unfiltered airspeed data
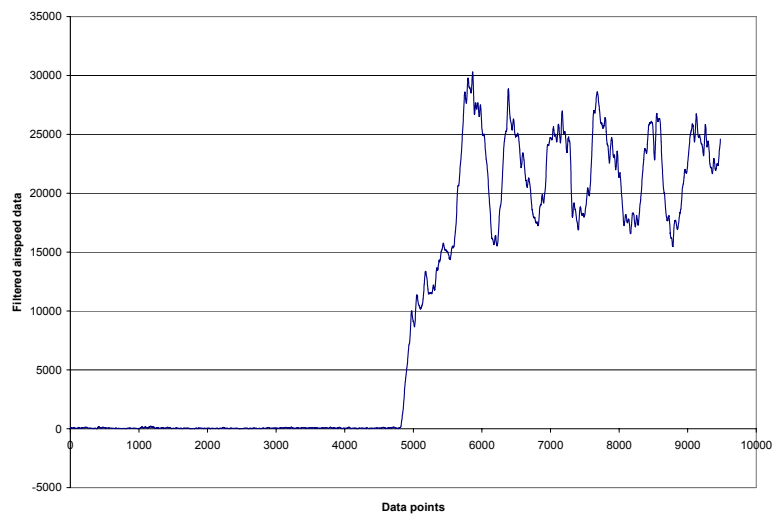
Figure III.6 Filtered airspeed data using low pass filter
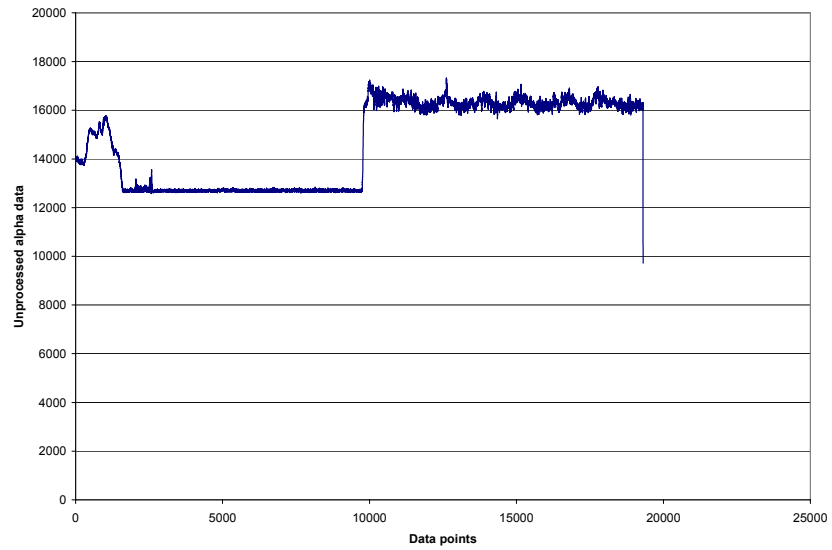
Figure III.7 Unfiltered α data
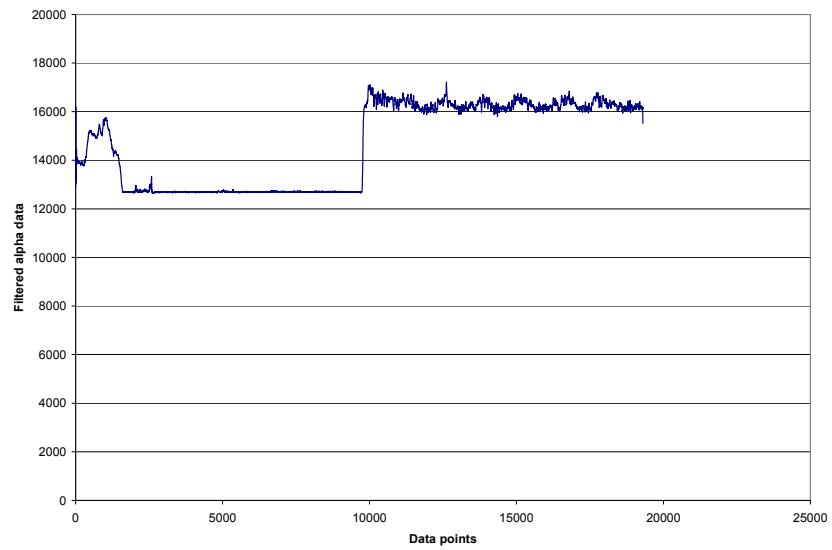
Figure III.8 Filtered α data using low pass filter

27
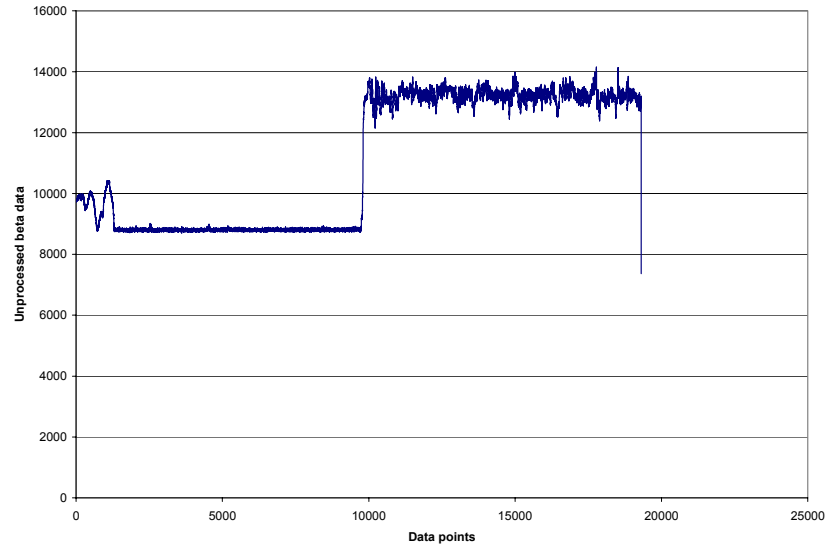
Figure III.9 Unfiltered β data
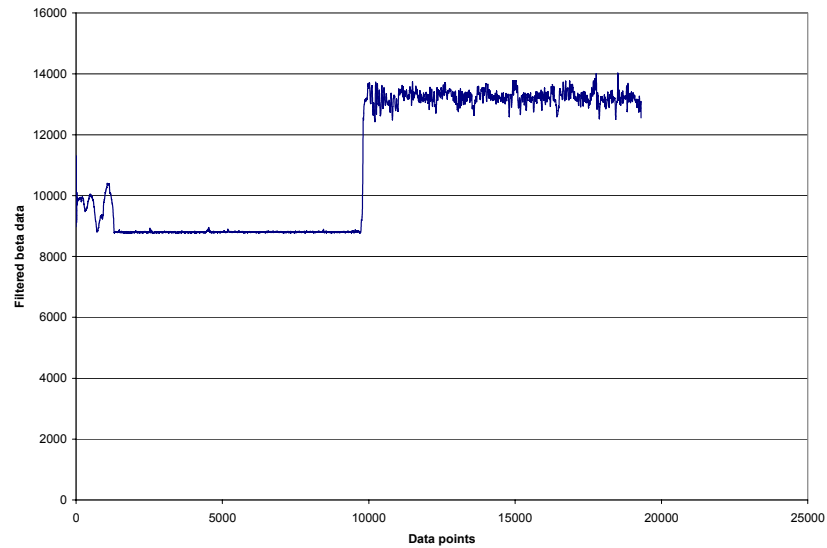
Figure III.10 Filtered β data using low pass filter

Figure III.5 and/or 6 shows the general idea of the test flight profile. The FROG take-off phase starts at about near the 5000th data point and six runway passes with turns were made (from the 6000th to 9500th data points). More

28

details of the flight maneuvers will be covered in Chapter IV.

It is distinctive from Figures III.5 through III.10 that the low pass filters (with the specified cut-off frequencies as mentioned in the above paragraph) were able to reduce the level of noise and enhance the fidelity of the air data.

C.   RESAMPLING

The air data system time tagging comes from the GPS clock which is streaming data at a frequency of 10 hertz. In order to ensure that analysis of air data is possible, it is necessary to have a common time history of the air data. This is particularly so for the airspeed and $\alpha-\beta$ data since these data were sampled at different frequencies from the GPS clock signal. The airspeed and $\alpha-\beta$ data were resampled using the MATLAB® 'interpft' function so as to achieve a common time history of the data. The 'interpft' function is a one dimensional interpolation using the FFT method. Figures III.11 through III.13 show the time histories of the filtered airspeed and $\alpha-\beta$ data; note the common time base of the data. Figures III.5 through III.10 show the x-axis of the plot to be data points whereas Figures III.11 through III.13 show the x-axis of the plot to be time now.
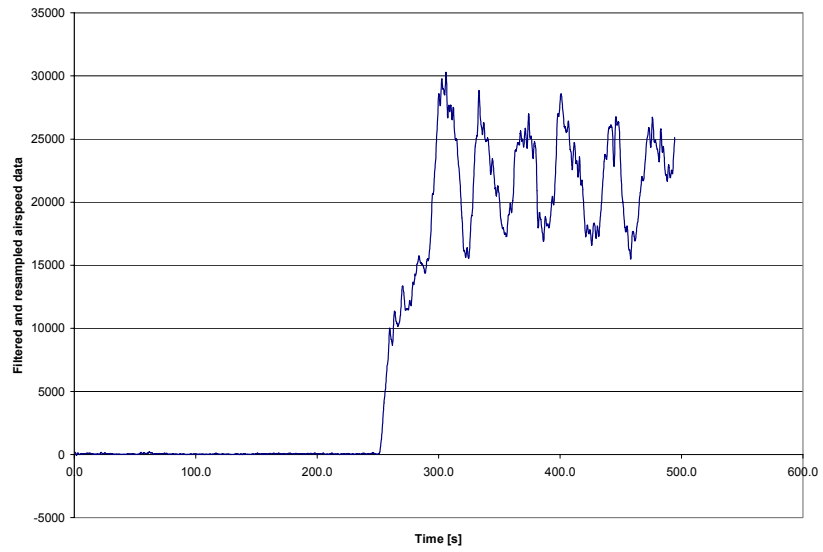
Figure III.11 Time history of filtered airspeed data
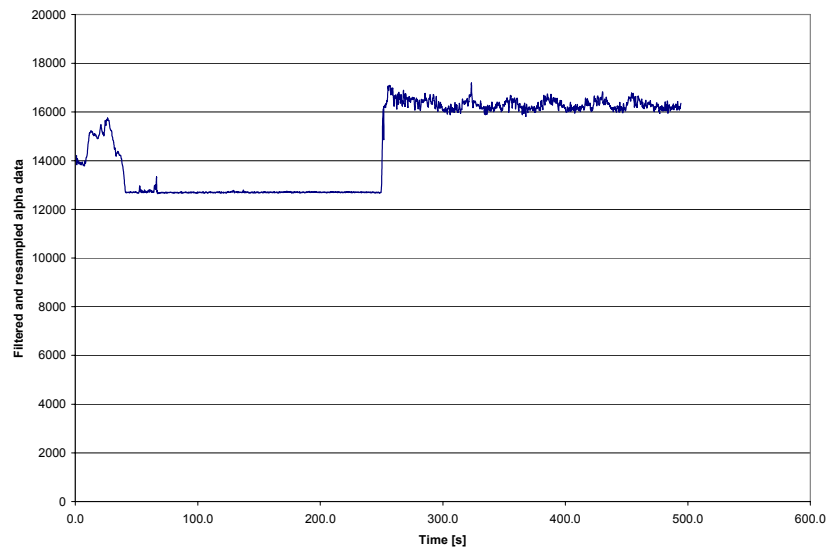
Figure III.12 Time history of filtered α data
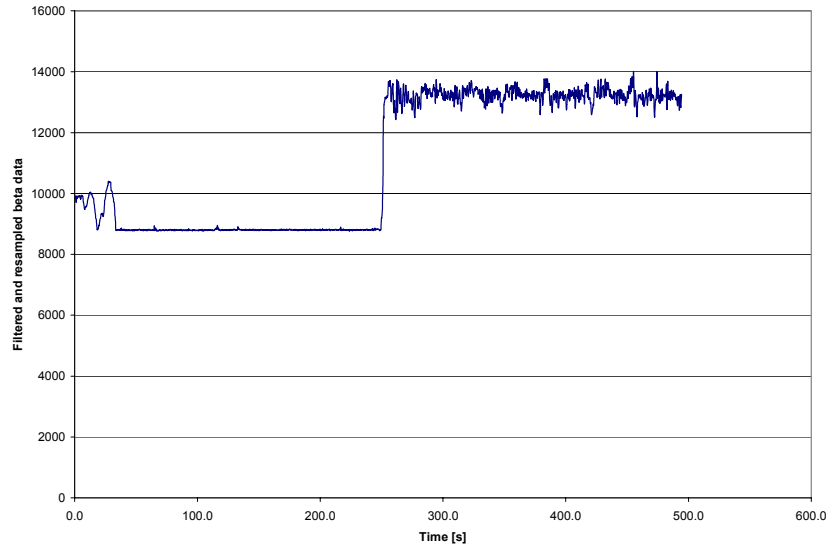
Figure III.13 Time history of filtered β data

D.   CALIBRATING

As mentioned in Chapter II section G, the calibration results (Equations (3) through (5)) were applied to the time history of the filtered air data. Figures III.14 through III.16 show the time history plots of the air data, filtered and calibrated with the proper desired units. Note that the airspeed determined is equivalent airspeed since the standard sea level density value was used in Equation (2).

31
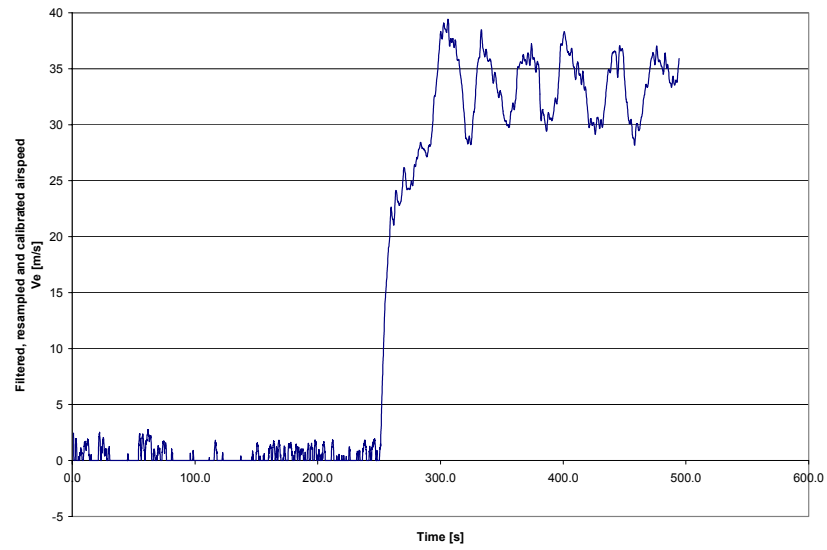
Figure III.14 Time history of filtered and calibrated
equivalent airspeed data
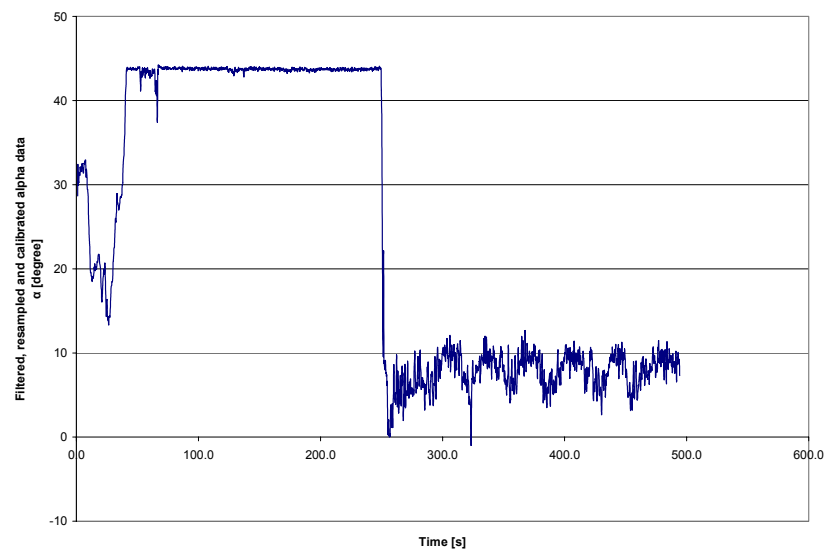
Figure III.15 Time history of filtered and calibrated α
data
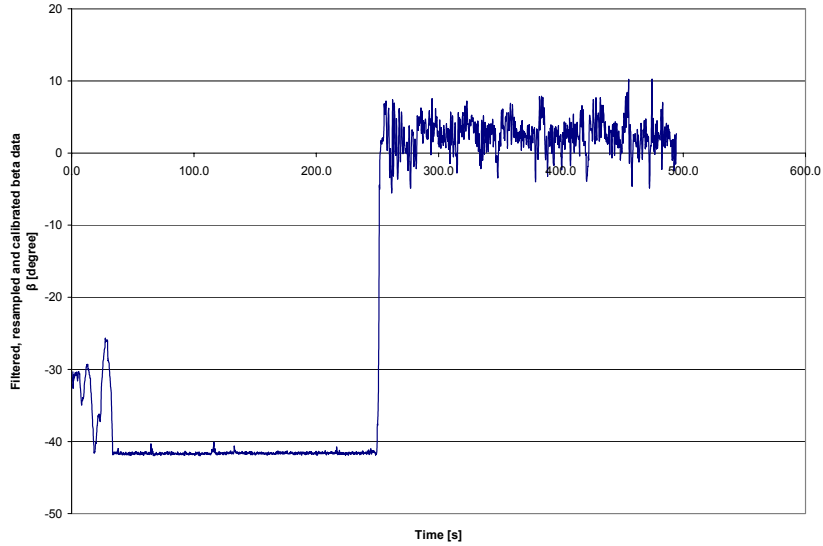
Figure III.16 Time history of filtered and calibrated β data

E.   STATIC AND DYNAMIC CORRECTION

The airspeed and $\alpha-\beta$ data have to be corrected for position errors, namely ΔV_{pc}, $\Delta\alpha_{pc}$ and $\Delta\beta_{pc}$ (static correction) and for induced pitch, roll and yaw rates (dynamic correction).

1.   Static Correction Through Off-Body Flow Analysis

The position error corrections were carried out using numerical simulation with a software suite, Personal Simulation Works (PSW[©]) from [4], which is comprised of LOFTSMAN, CMARC and POSTMARC. PSW[©] is based on inviscid potential flow analysis and it provides for panel model development, input file processing and the visualization of results. Appendix C gives details of the software suite PSW[©]. Figure III.17 shows the numerical model of the FROG for this thesis work. This numerical model was generated

after modification of a previous CMARC simulation carried out by the author of [4] so that position errors can be computed for the wing tip installations of the pitot-static and $\alpha - \beta$ probes. The CMARC source code for numerical simulation can be found in [4].
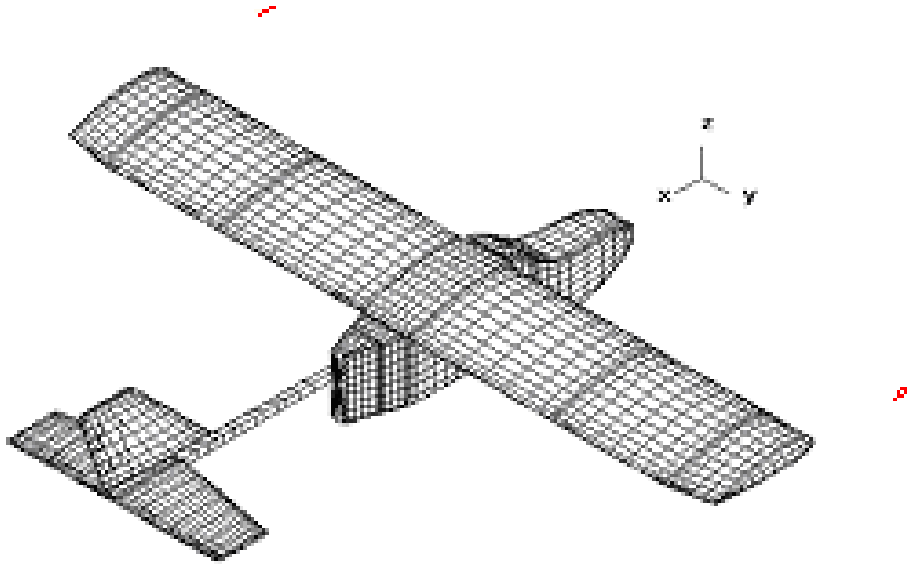
Figure III.17 CMARC numerical model of the FROG.

CMARC is ideally suited for off-body flow analysis. Note the off-body streamlines in Figure III.17. Off-body streamlines may be placed through a point anywhere in the flow field. CMARC will then follow the streamline up and downstream the distance designated in the input file. This is particularly useful for flow visualization. In addition, CMARC calculates the pressure coefficient and velocity at each point along the streamline. For this thesis, one streamline was placed through each of the following locations: static pressure source, α and β vanes. The pressure coefficient (from CMARC) is used to calculate the

34

static source position error while the velocity vector (from CMARC) is used to calculate both α-β probe position errors (a strong function of α and β respectively).

a.   Analysis of Static Source Position Error

The position error pressure coefficient, ΔC_{p-pc} or $\Delta Pp/q_c$, is a function of free stream Mach number and α provided that the static source is located outside of a thick boundary layer and sideslip is minimized (from [5]). In the case of the FROG which is in incompressible flow, $\Delta Pp/q_c$ becomes only a strong function of α and it is basically independent of airspeed and altitude.

The CMARC numerical simulation was carried out; Figure III.18 shows the variation of the position error pressure coefficient against indicated α. The second order influence of α is clear with a second order curve fitting tightly through the data points.
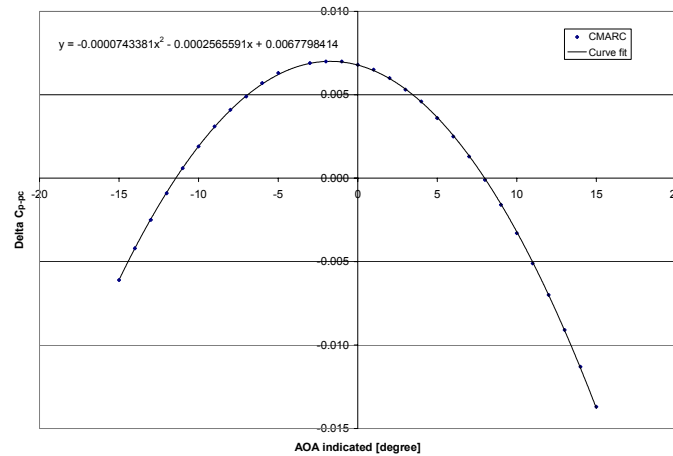
Figure III.18 Position error pressure coefficient, ΔC_{p-pc}

Position error pressure coefficient can be turned into position corrections for airspeed and altitude. The following relations were developed which assumed small errors and incompressible flow:

$$\Delta V_{pc} = \frac{V_i \Delta C_p}{2} \quad \text{and} \quad \Delta V_{pc} = V_c - V_i \tag{6}$$

$$\Delta H_{pc} = \frac{V_i \Delta V_{pc}}{\sigma_{std} g_o} \quad \text{and} \quad \Delta H_{pc} = H_c - H_i \tag{7}$$

Where:

ΔH_{pc} = altitude position correction

ΔV_{pc} = velocity position correction

ΔC_p = position error pressure coefficient

σ_{std} = standard day density ratio

g_o = gravitational constant

The velocity position correction was applied to the airspeed data. Figure III.19 shows the variation of V_{pc} with indicated α while Figure III.20 shows the time history of filtered, calibrated and statically corrected airspeed data of the FROG. Note the slight difference in the magnitude of the airspeed in this figure and Figure III.14.

36
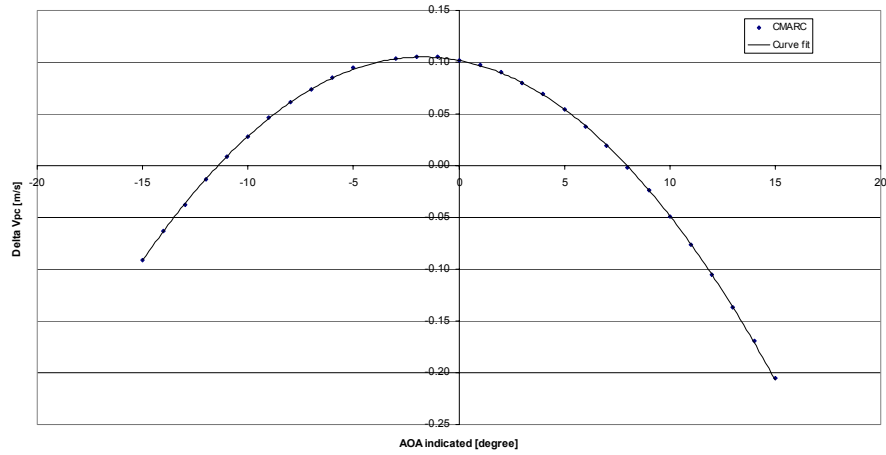
Figure III.19 V_{pc} variation with indicated α
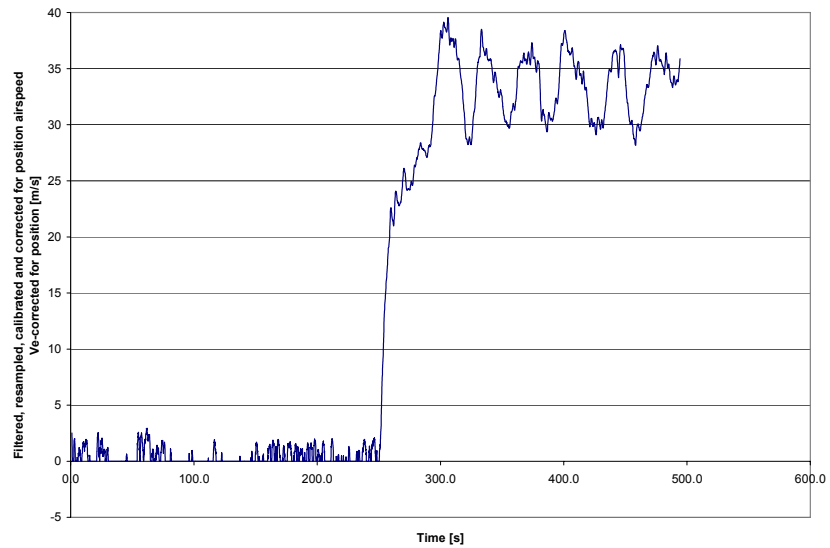
Figure III.20 Time history of filtered, calibrated and
statically corrected airspeed data

b.   *Analysis of Alpha Vane Position Error*

Local flow field velocity was extracted from the
off-body streamline listing to obtain the local α. The α
vane was assumed to capture the x-z component of the local
velocity field and ignore cross flow in the y direction.

37

The flow field velocity was turned into indicated α and α-position correction with the following equations:

$$\alpha_i = \tan^{-1}(\frac{V_z}{V_x}) \quad \text{and} \quad \Delta\alpha_{pc} = \alpha_t - \alpha_i \qquad (8)$$

Figure III.21 shows the $\Delta\alpha_{pc}$ as a function of indicated α as it was derived from CMARC off-body flow field analysis. The α correction is fairly linear throughout the FROG operating envelope and the corrections apply at all incompressible airspeeds and altitudes. Figure III.21 was used to correct the α data of the FROG. Figure III.22 shows the time history of filtered, calibrated and statically corrected α data of the FROG.

Figure III.21 α vane position error, $\Delta\alpha_{p\text{-}pc}$, for the FROG.

38
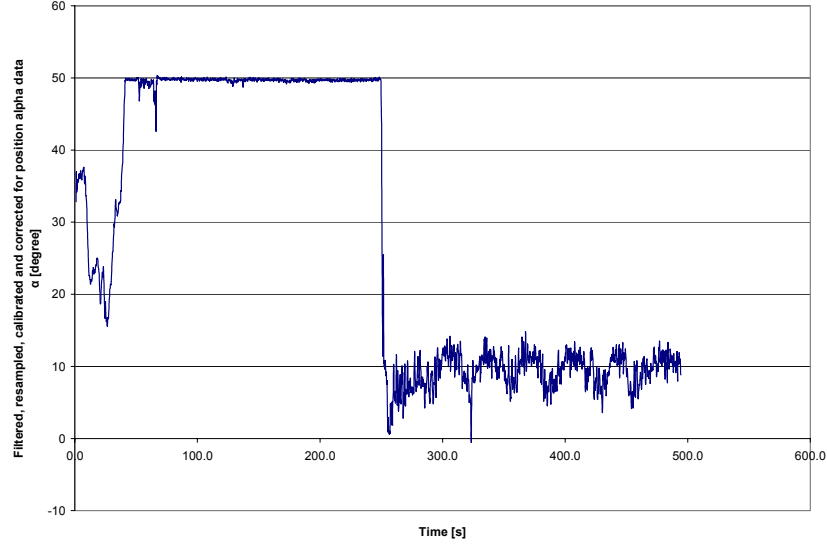
Figure III.22 Time history of filtered, calibrated and statically corrected α data

c.   Analysis of Beta Vane Position Error

Local flow field velocity was similarly extracted from the off-body streamline listing to obtain local β angle. The beta vane was assumed to capture the x-y component of the local velocity field and ignore vertical flow in the z direction. Flow field velocity was turned into indicated β and β position correction with the following equations:

$$\beta_i = \tan^{-1}(\frac{V_y}{V_x}) \quad \text{and} \quad \Delta\beta_{pc} = \beta_t - \beta_i \tag{9}$$

Figure III.23 shows the $\Delta\beta_{pc}$ as a function of indicated β. The β correction is fairly constant throughout the FROG operating envelope and the corrections apply at all incompressible airspeeds and altitudes. Figure

39

III.23 was used to correct the β data of the FROG. Figure III.24 shows the time history of filtered, calibrated and statically corrected β data of the FROG.
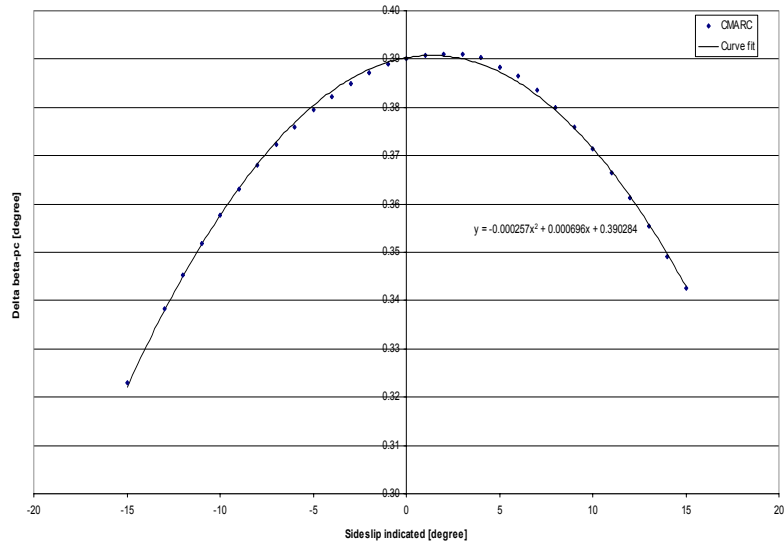
Figure III.23 β vane position error, $\Delta\beta_{p-pc}$, for the FROG
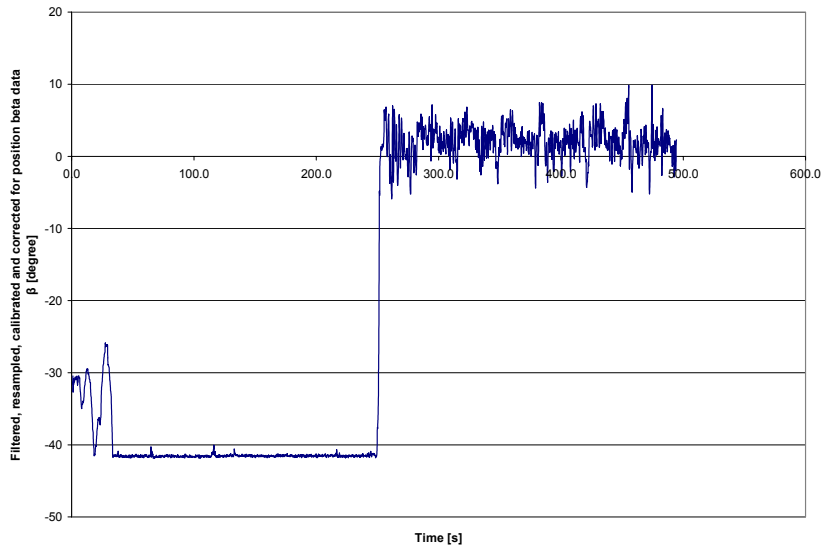
Figure III.24 Time history of filtered, calibrated and statically corrected β data

2.   Dynamic Correction for α and β

Since the α-β probe is not located at the CG position of the FROG, there is a need to correct the α-β data due to induced roll, pitch and yaw rates. From [6], the correction equations are as follows:

$$\alpha_{corrected} = K_\alpha(\alpha_{indicated} - \frac{x_\alpha}{V}q + \frac{y_\alpha}{V}p)$$

$$\beta_{corrected} = K_\beta(\beta_{indicated} - \frac{z_\beta}{V}p + \frac{x_\beta}{V}r) \tag{10}$$

Where:

Kα and Kβ are upwash factors on α and β respectively

p, q and r are the roll, pitch and yaw rates respectively

x, y and z are the positions of the α-β probe relative to the aircraft CG in accordance with the coordinate system as shown in Figure III.25.
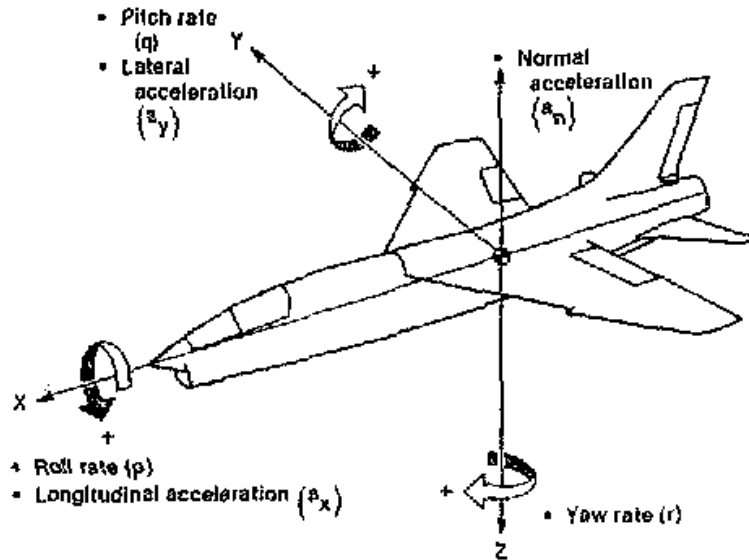
Figure III.25 Coordinate system for dynamic correction to air data (From [6])

The application of the upwash factors is debatable and the effect is of second order (as mentioned in [6]). As such, for this dynamic correction, a value of 1 was selected for Kα and Kβ. With the dynamic corrections being carried out, the values of α-β are those of true values. Figures III.26 and III.27 show the time histories of the complete and processed true values of α and β respectively.
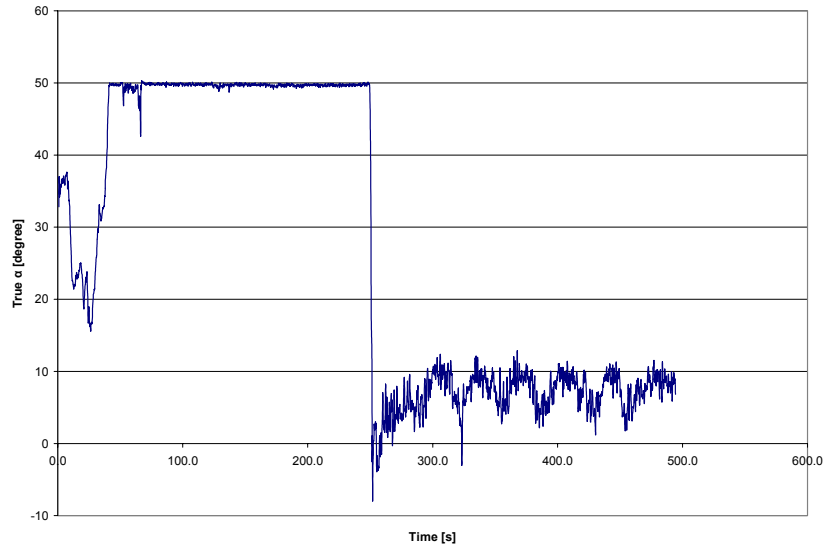
Figure III.26 Time history of true α
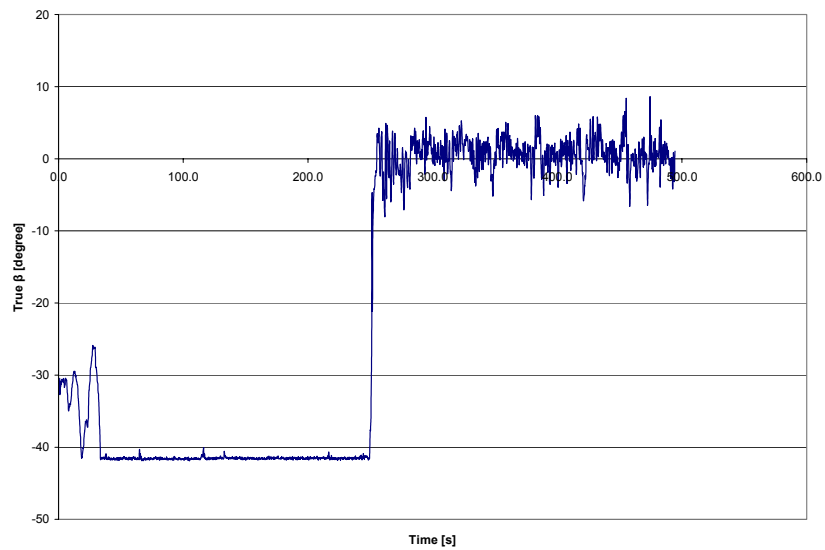
Figure III.27 Time history of true β

3.   Density Correction for Airspeed

The last required air data correction is the density correction for airspeed since density varies with location and altitude. The meteorological data from the weather

balloon showed that density did not varied much from ground level to the altitude of the flight profile on the day of the test flight (since the FROG was flying at low altitude). The average density determined from the meteorological data was 1.182654 kilograms per cubic meter and this value was used to correct the processed airspeed to get the final, complete true airspeed. Figure III.28 shows the true airspeed of the FROG.
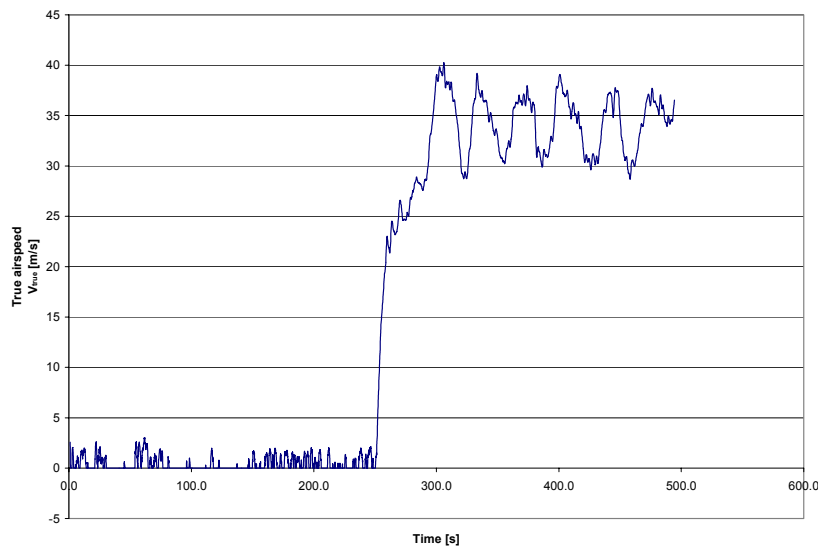
Figure III.28 Time history of true airspeed

F.   WIND DATA EXTRACTION

As mentioned in the objectives, the motivation is to have a successful response to a Chem/bio attack which in turn involves measuring and predicting the dispersion of a toxic agent in the atmosphere. The dispersion of the toxic agent is dependent on the wind velocity in the atmosphere. Hence, wind estimation will enable dispersion prediction of

44

the toxic agent. Wind estimation is based on the following fundamental velocity vector equation:

$$^{i}V_{w} = {}^{i}V_{b,i} - {}_{w}^{i}RV_{b,w}$$ (11)

Where:

$^{i}V_{w}$ is the wind vector in the inertial coordinate system

$^{i}V_{b,i}$ is the FROG velocity in inertial coordinate system obtained from the GPS unit onboard the FROG

$_{w}^{i}R$ is the rotation transformation matrix from wind to inertial coordinate system

$V_{b,w}$ is the FROG velocity in the wind coordinate system obtained from the pitot-static probe

A Simulink® model (from MATLAB®) was created in [9] to extract the wind data. The Simulink® model fundamentally is based on the above mentioned equation and it takes in air data and computes the necessary $_{w}^{i}R$, which is the rotation matrix to the inertial coordinate system, so that wind extraction can be carried out. Figure III.29 gives a preview of the schematic of the Simulink® model.
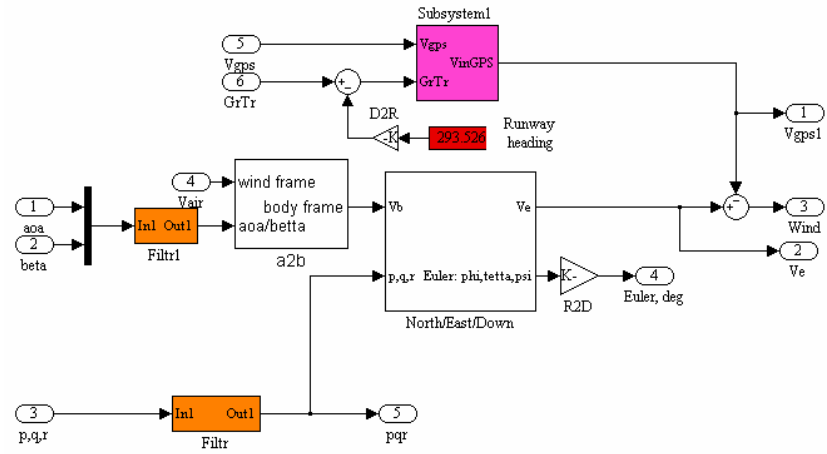
Figure III.29 Preview of Simulink® model for wind extraction (From [9])

IV AIR DATA ANALYSIS

A.   ANALYSIS OF AIR DATA

1.   True Airspeed

Figure IV.1 shows the true airspeed, GPS ground speed and altitude (MSL) level of the FROG during the test flight as mentioned in Chapter III Section A. Specific legs during the test flight were identified and are as indicated in the figure. The magnitude of the wind vector can be estimated from this figure. The difference between the true airspeed and GPS ground speed, i.e., the difference between the blue and pink lines, is the estimated ballpark wind vector magnitude; which in this case shows that the wind magnitude during the test flight was no more than 10 meters per second. This is incorrect from a strict point of view, since the actual wind vector magnitude has to be computed as mentioned in Chapter III Section F.

The FROG started its take-off run at about time = 250 seconds. Prior to that, the FROG was on the taxiway being checked out for its functionality. From the altitude curve, it was evident that the FROG lifted off from the runway at time = 253.3 seconds. The aircraft started to climb and made a right turn followed by a left turn to line up for the first pass of the runway. A total of six runway passes were made. The duration, average speed and altitude (MSL) level for each pass was approximately 10 seconds, 38 meters per second and 300 meters respectively. Each time after a pass, the FROG turned left to line up for the next pass. In the first part of the turn, the FROG was climbing from an

47

altitude (MSL) of 300 to 320 meters and losing its airspeed
from 38 to 30 meters per second at the same time. As the
FROG completed each turn (second part of turn) to line up
for the runway pass, it descended from an altitude (MSL)
320 to 300 meters and regained its airspeed back to 38
meters per second.
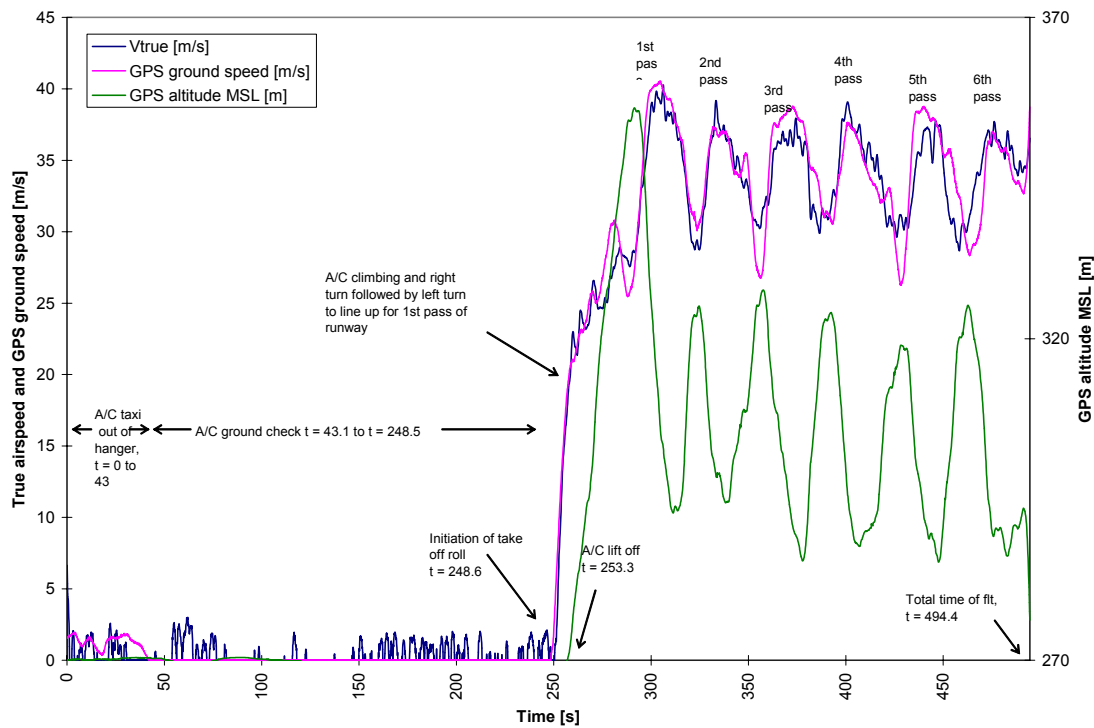
Figure IV.1 True airspeed correlated with test flight
profile

The pilot of the FROG did confirm that the FROG
was indeed performing the above mentioned maneuvers. Hence,
the airspeed data was concluded to be sensible and valid.

48

2. True $\alpha - \beta$

Figure IV.2 shows the true $\alpha - \beta$ of the FROG. Note that the figure only shows the true $\alpha - \beta$ after the FROG had lifted off from the runway, i.e., from time = 250 seconds, for the sake of clarity. The runway pass is as indicated in the figure. The first observation to be made from the figure is that the α was always positive throughout the time which the FROG was airborne. This makes sense since the FROG was not expected to fly at negative α. The second observation is that the β fluctuated between ± 5° most of the time. This also makes sense as the pilot was constantly making rudder and/or aileron input to prevent the FROG from flying in a 'crab like' manner.
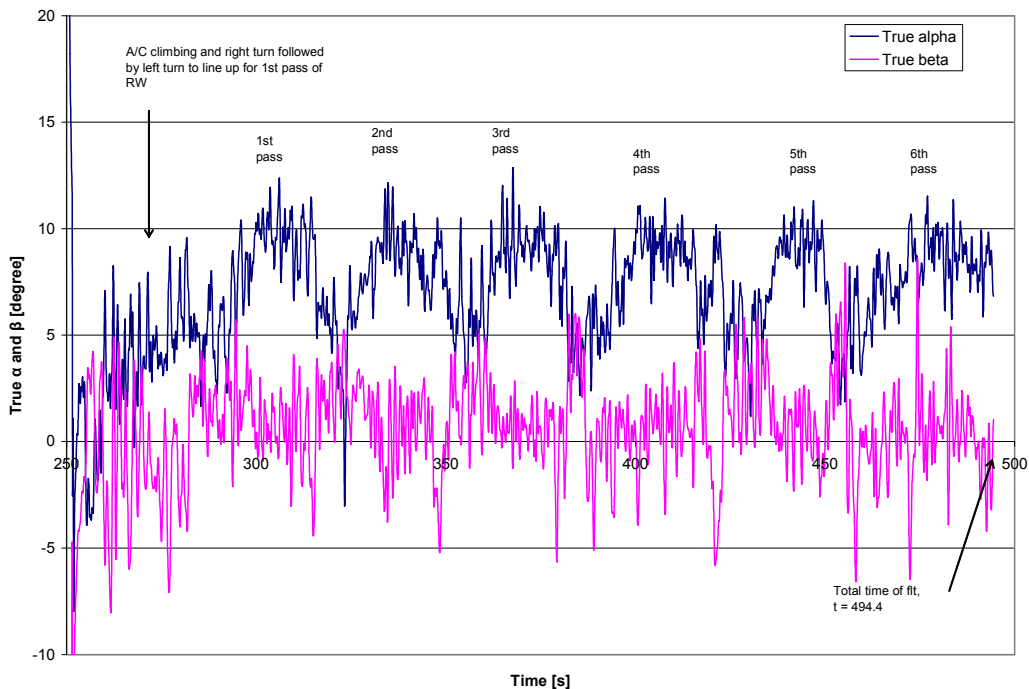
Figure IV.2 True $\alpha - \beta$ correlated with test flight profile

49

As mentioned in the previous section, the FROG turned left in between runway passes and each turn was comprised of a climb with decreased airspeed followed by a descent with increased airspeed. As the FROG initiated each left turn (climb and decreased airspeed), the α decreased from approximately 10° to 5° while the β increased from approximately 0° to 5°. The completion of the left turn (descent and increased airspeed) was achieved with α increasing from 5° to 10° and β decreasing from 5° back to 0°. Since β was defined as positive when 'wind in right ear' which implied a left turn, this is consistent with the data presented. Note that during the duration of the runway passes, β fluctuated between ± 3° which was evidence of the FROG compensating to fly straight along the runway passes.
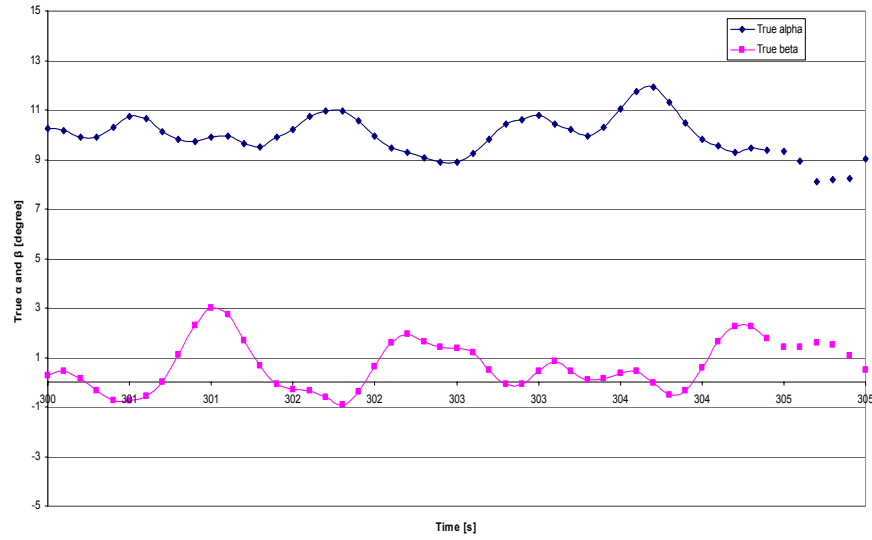
Figure IV.3 Sample close-up of true α-β

Figure IV.3 shows a sample close-up of true α-β with the data points from time, t = 300 to 305 seconds. Note the

closely 'packed' data points, indicating that the data points represent actual data, not high frequency noise.

THIS PAGE INTENTIONALLY LEFT BLANK

V POSSIBLE IMPROVEMENTS TO AIR DATA SYSTEM

A. PRESSURE TRANSDUCER COMPARISON

The pressure transducer that was used on the FROG (for ease of identification, it is named as transducer A) was compared to another type of transducer; transducer B. Appendix D documents the detailed data specifications of transducer B. A wind tunnel experiment was conducted to compare both transducers.

1. Wind Tunnel Experiment

The wind tunnel experiment was conducted with a pitot-static probe mounted in the wind tunnel to measure dynamic pressure. The dynamic pressure was given as input to both transducers at the same time so that the quality of the output signals from both transducers can be compared. Both of the transducers output signals were processed by a processor with a 12-bit analog to digital converter which was sampling data at a frequency of 40 hertz. The first part of the experiment involved operating the wind tunnel at different speed settings while the second part involved operating the wind tunnel at a particular speed setting but subjecting both transducers to vibration.

2. Wind Tunnel Experiment Results

Figure V.I shows the raw output signal of both pressure transducers from the first part of the experiment. The step-like shape of the curve is due to the different wind tunnel speed settings carried out during the first part of the experiment. The magnitude of the signal is not

important but rather the fluctuation of the signal at a particular voltage is of importance since that translates to the noise level of the transducer which in turn determines the quality of the transducer. Although both signals from Figure V.1 look almost the same in terms of shape, upon careful scrutiny, the blue signal shows obviously that transducer B is of better quality as the noise level or signal fluctuation is less than that of transducer A. This is evident from Figure V.2 which shows a close-up of the output signals from both transducers from the 50th to 100th data point at the same scale. A PSD plot is carried out for both transducers to further verify the noise level and the frequency content of both signals. Figures V.3 shows the PSD plots of both transducers.
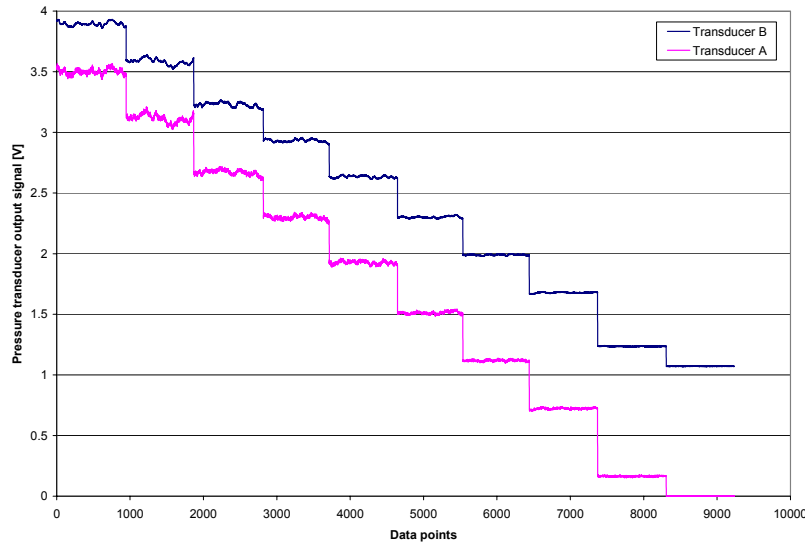
Figure V.1 Output signals of transducer A and B during first part of wind tunnel experiment

54
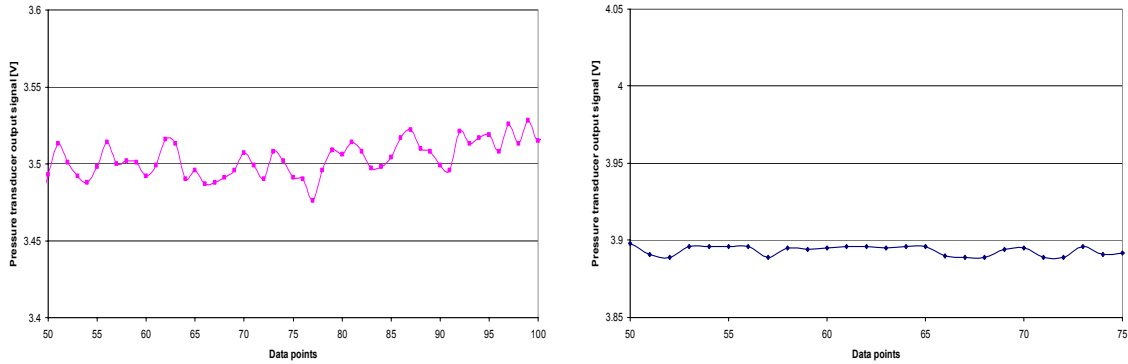
Figure V.2 Sample close-up of output signals of transducer A (left) and B (right) from 50th to 100th data point

Figure V.3 was produced from the first part of the wind tunnel experiment (different wind tunnel speed settings). Note that Figure V.3 shows a lot of peaks in the range of 6 hertz and above, evidence of the fact that the noise associated with the transducers are of frequencies of 6 hertz and above. The peaks in the region of less than 2 hertz for both plots show the fundamental frequency of the signal (dynamic pressure) being measured. The fact that the PSD curve for transducer A is of a higher value than that of transducer B points to the fact that transducer A output signal contains more noise.

55
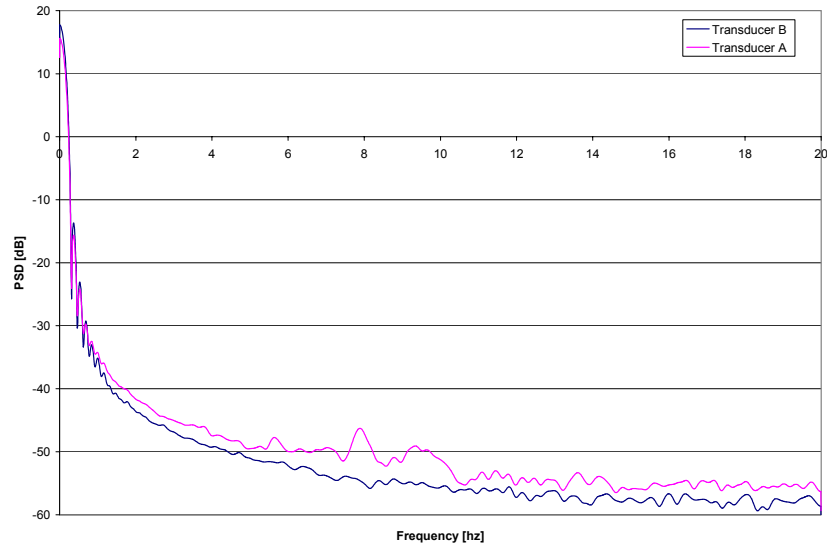
Figure V.3 PSD plot of transducer A and B

The second part of the wind tunnel experiment involved analyzing the signals from the transducers by subjecting the transducers to external vibration. The mass elements inside the pressure transducers respond to vibration as accelerometers, another noise source. The vibrations were generated from a Siemens S40 cell phone. This was done to simulate the vibrations that the transducers would encounter when installed onto the FROG. Figure V.4 shows both the output signals of the transducers with both transducers subjected to vibrations while Figure V.5 shows a sample close-up of the signals from the 450th to the 500th data point. Note the obvious noisy signal and the relatively large signal fluctuation produced by transducer A.

56
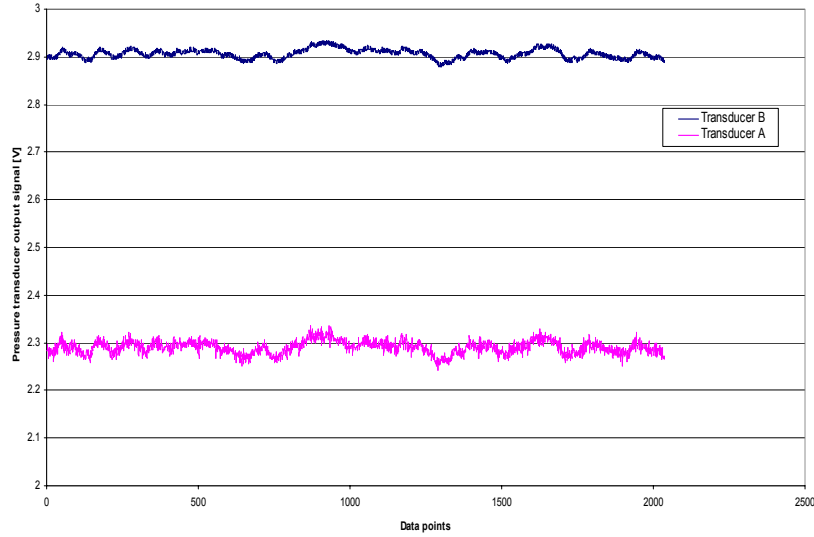
Figure V.4 Output signal of transducer A and B during second part of wind tunnel experiment
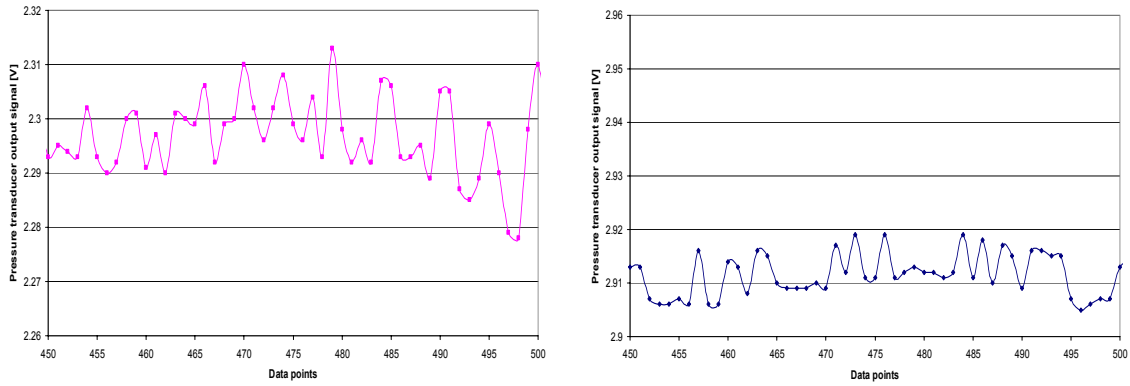
Figure V.5 Sample close-up of output signals of transducer A (left) and B (right) from 450th to 500th data point

Similarly to the first part of the wind tunnel experiment, a PSD plot was carried out for both transducers to further verify the noise level and the frequency content of both signals. Figure V.6 shows the PSD plots of signals from both transducers subjected to vibrations. Comparing with the PSD plot in Figure V.3, there are a lot more peaks

this time due to the fundamental vibration frequencies. Note how noisy the transducer A is compared to transducer B. Compare the peaks from the range of more than 2 hertz.
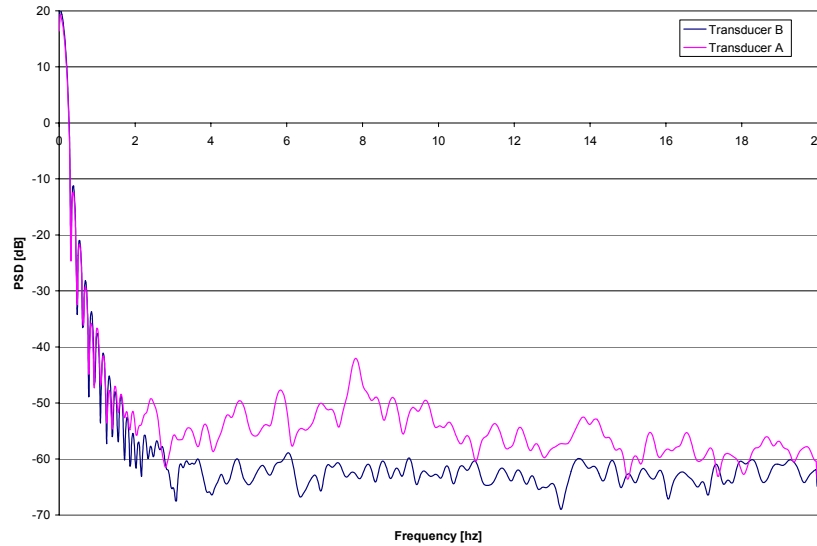
Figure V.6 PSD plot of transducer A and B

Figures V.1 through V.6 clearly suggest the fact that transducer B is of a better quality in terms of noise production.

B.   MULTI-HOLE PROBE

Fluid mechanics have employed a variety of single and multi-hole probes in research and design. The most common is the well-known pitot static tube which is used on the FROG, while another single-hole probe is the Preston tube, which is practically a flattened-down pitot tube. Multi-hole probes have also been used extensively to provide velocity magnitude and direction with high accuracy for angles as high as 75° for standard five and seven-hole

58

probes, and 165° for omni-probes. Multi-hole probes are designed to determine velocity through direct measurement of the pressures at the probe tip and then using the pressures to calculate the velocity. These probes provide point measurements of the flow velocity vector and the total and static pressure with minimal interference to the flow.

Alternative tools for point measurements in a flowfield are the hot-wire anemometer and the Laser-Doppler Velocimeter. A quick comparison of the advantages and disadvantages of the three main tools are as follows (extracted from [7]):

Hot-Wire Anemometry

A hot-wire anemometer imposes low interference on the flow and provides the highest possible frequency response. On the other hand, it requires often and tedious calibration and frequent repairs of damaged wires. Moreover, to generate more than one component of the velocity, one has to use multiple wires, which are sensitive, fragile and hard to calibrate.

Laser-Doppler Anemometry

This method relies on the processing of laser light scattered by micro-scale particles moving with the flow. Since the technique is optical, it presents no interference with the flow. It does not require calibration but the user must seed the flow. Seeding is a tedious and not always

successful procedure. Moreover, positioning of the measuring volume in the desired location is not easy.

Multi-Hole Probe System

A multi-hole probe is rugged. It requires only one calibration at the end of its manufacturing process. Its use is very simple and the technique can provide information on all the primitive variables of the flow.

Table V.1 shows the comparison matrix of each main method of measurement including the pitot-static probe system.

Table V.1 Comparison of Different Measurement Technique

	Hot-Wire Anemometry	Laser-Doppler velocimeter	Multi hole probe system	Pitot-static probe + alpha beta vane system
Calibration	Often	None	Once	Once
Interference	Low	None	Low/Medium	Low/Medium
Signal	Continuous	Discrete	Continuous	Continuous
Frequency response	High	Medium	Medium	Medium/Low
Difficulty of operation	Medium	High	Low	Very low
Cost	Medium	High	Low	Very low
Accuracy	High	High	High	Medium/Low
Use on FROG	Almost impossible	Impossible	Very possible	Very possible

1. 5-Hole Probe

A 5-hole probe was custom made as part of this thesis search for better air data sensors onboard the FROG. The 5-hole probe is expected to be more precise and accurate in measurement of $\alpha - \beta$ angles compared to using the vanes mounted on the pots. Figure V.7 shows the dimensional drawing of the 5-hole probe.
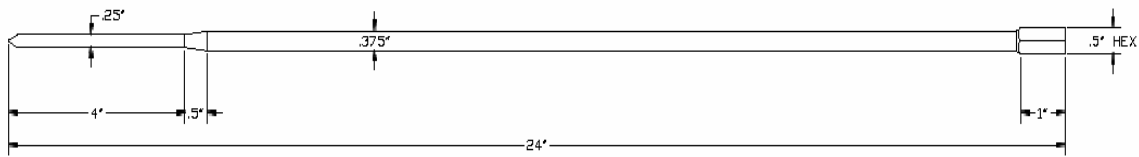
Figure V.7 Dimensional drawing of 5-hole probe

The construction of probes can be divided into the fabrication of internal and external features. The external features define the geometry exposed to the flow. The internal features define the discreet pressure channels that transmit the pressure from the probe tip to the pressure transducers.

a. External Features

Figure V.8 illustrates the arrangement of the probe components. Probe tips are typically made of brass or stainless steel. There are three parameters defining the tip geometry and features: tip diameter, shape (conical, hemispherical, and faceted) and number of holes (5 or 7). The first extension (Figure V.8) precisely matches the

outside diameter of the tip and is typically up to 20 tip diameters long. Ferrules gradually increase the outside diameter of the probe shaft, providing the strength of material necessary for a given length. If needed, a second extension can be added, creating a longer shaft. A third extension can also be added if needed, creating a very long probe for special applications. Mounts are typically hexagonal to allow for probe roll referencing.
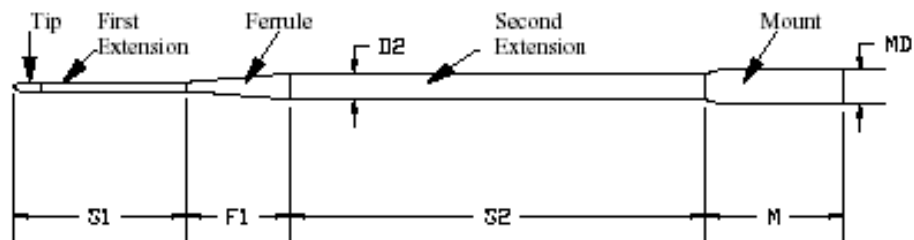
Figure V.8 Typical layout of 5-hole probe
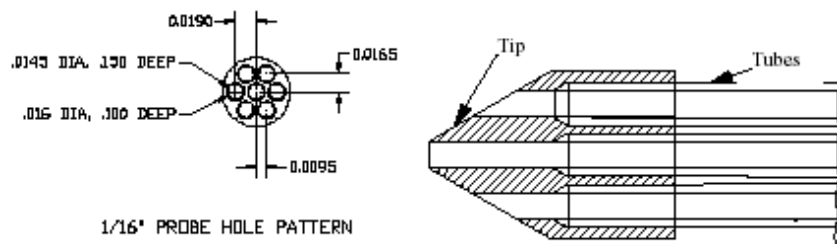
Figure V.9 Details of 5-hole probe tip

b.   *Internal Features*

Each of the holes in the probe tip leads to a stainless steel tube, with its inside diameter matching the diameter of the hole. As the probe shaft diameter increases, each tube is telescoped into a larger tube,

62

which finally protrudes from the back of the mount. Each connection is soldered and tested for strength and leakage. The final assembly is also tested for pressure "cross-talk", i.e. pneumatic communication between two or more probe holes and their associated tubing. Figure V.9 presents structural details of a typical probe tip and sample dimensions for a 0.062" (1/16") tip diameter probe tip.

2.   Principle of Operation for Multi-Hole Probe

The pressure over a bluff body is the highest at the stagnation point and lowest near separation. If the flow direction forms small angles with the axis of the probe (below 20°), the center hole registers the highest pressure. If however, the flow is steeply inclined with respect to the probe, as shown in Figure V.10 for a seven-hole probe, then one of the peripheral holes on the windward side of the probe tip registers the highest pressure, while on the leeward side of the probe, the flow is separated. The pressure information provided by the three holes in the separated region is not used. Careful calibration can thus allow the instrument to measure the direction and the magnitude of the velocity.
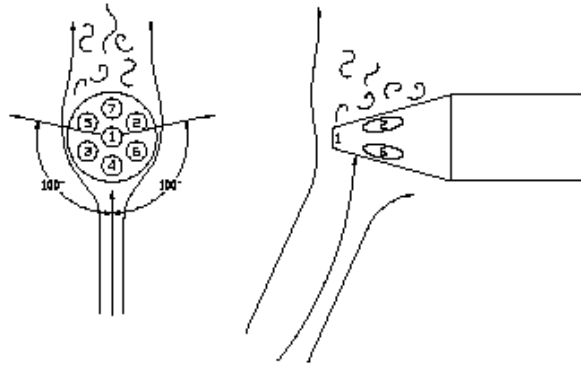
Figure V.10 Multi-hole probe inserted in flowfield

Using the 5-hole probe to measure α and β is governed by the following simplified basic principle: Defining the port pressure as per Figure V.11, ΔP is defined as $\dfrac{(P1 - P_{avg})}{P1}$ where $P_{avg} = \dfrac{(P2 + P3 + P4 + P5)}{4}$. Therefore, α is proportionate to $\dfrac{(P4 - P5)}{\Delta P}$ whereas β is proportionate to $\dfrac{(P2 - P3)}{\Delta P}$ and it is this proportionality that allows the $\alpha - \beta$ to be determined once the calibration is carried out.
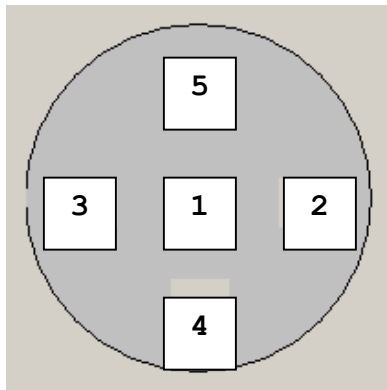
Figure V.11 Typical 5-hole probe port numbering system

Due to the finite size of the probe (and the very nature by which it operates), one may anticipate some interference with the flow. Caution should be exercised if one attempts to measure too close to a solid wall and in boundary layers. Fluid mechanics phenomena that are very sensitive to external disturbances have also been known to be affected by the probe. For example, inserting the probe near the core of a columnar vortex, like the tip vortex of a wing, may induce vortex breakdown and inserting the probe in a laminar shear layer or a laminar boundary layer at moderate Reynolds numbers may induce transition.

3.   Wind Tunnel Experiment

A wind tunnel experiment was conducted to compare the $\alpha-\beta$ data acquired by 5-hole probe-transducer and $\alpha-\beta$ vane-pots systems. Both probes were mounted in the wind tunnel (which has a flow turbulence level of 0.23%) to measure only β since measuring β alone is sufficient for a comparison of the two measurement systems. Figure V.12 shows how both the probes were mounted in the wind tunnel section. The free-stream velocity of the tunnel was set to approximately 25 meters per second since the FROG operating speed range is 25 - 35 meters per second. The output signals from the five pressure transducers (Transducer B type) and the signals from the β pot were processed by a processor with a 10-bit analog to digital converter which was sampling data at a frequency of 40 hertz.

65

Figure V.12 Set-up of β vane-pot and 5-hole probe-
transducer system

Prior to the experiment, the β pot and the transducers were calibrated the same way as it was done for the FROG as mentioned in Chapter II. The first part of the experiment involved operating the wind tunnel at a specific speed setting and measuring β from $-8°$ to $+12°$ at intervals of $2°$ statically while the second part involved measuring β from $-10°$ to $+12^0$ dynamically. Since five transducer B types were used in the experiment, the port pressures (P1, P2, P3, P4 and P5) were all referenced to atmospheric pressure. The pressure values were reduced to compute the β values using a calibration software, Multiprobe[©]. Note that Multiprobe[©] produces many parameters of interest: α-β, u-v-w components of velocity, total velocity V, total pressure and static pressure and total temperature and static temperature.

The β vane-pot system was mounted on a turn-table as shown in Figure V.12. The zero β reference was obtained by aligning the probe to be parallel to the wind tunnel and the β vane to be parallel to the airstream. The probe alignment was done visually; standing in the middle of the wind tunnel and adjust the turn-table till the probe is aligned. Once the probe was aligned, the vane was aligned by running the wind tunnel up to speed and let the airstream align the vane. Once that was done, the turn-table angular scale was reset to zero as reference. Subsequently, as β was measured in intervals of 2°, it was based on the turn-table angular scale.

4.   Wind Tunnel Experiment Results

Results obtained from the first part of the experiment are as shown in Figure V.13. From Figure V.13, it can be assessed that both systems of β measurement were in reasonably close agreement although there were slight differences between the β values especially at higher β value.

67
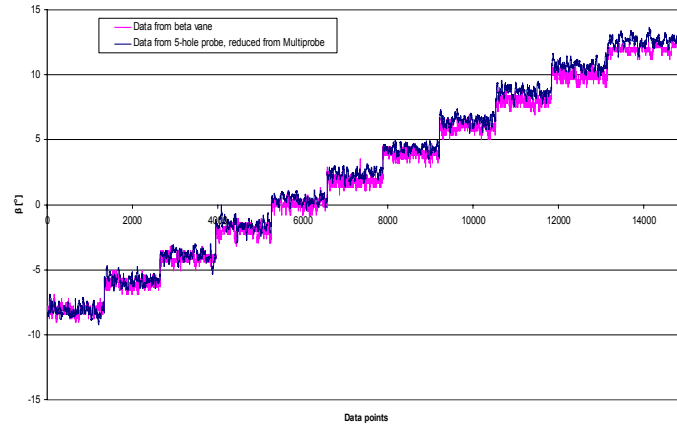
Figure V.13 Static measurement of β from 5-hole probe and β pot

Table V.2 summarizes the mean and RMS values of the signal from the β vane-pot and 5-hole probe-transducer system. Since the β vane-pot readings were used as reference (the visual alignment in the wind tunnel was taken as zero for the beta vane-pot system), the mean values were corrected so that a better comparison can be made. Table V.3 shows the corrected mean and difference values as well as the RMS values of the signals from both systems.

Table V.2 Mean and RMS values from β vane and 5-hole probe

Mean value from β vane	Mean value from 5-hole probe	RMS value from β vane	RMS value from 5-hole probe
-8.10	-8.12	0.29	0.38
-6.02	-5.82	0.29	0.38
-4.09	-3.89	0.26	0.42
-1.94	-1.56	0.34	0.39
0.06	0.42	0.29	0.31
1.86	2.39	0.29	0.33
3.91	4.31	0.28	0.29
5.96	6.46	0.29	0.36
8.01	8.67	0.27	0.37
9.94	10.69	0.30	0.36
12.01	12.61	0.27	0.35

Table V.3 Corrected Mean and RMS values from β vane and 5-hole probe

Tunnel reference	Corrected mean value from β vane	Corrected mean value from 5-hole probe	Difference	RMS value from β vane	RMS value from 5-hole probe
-8.00	-8.16	-8.18	-0.02	0.29	0.38
-6.00	-6.08	-5.88	0.20	0.29	0.38
-4.00	-4.15	-3.95	0.21	0.26	0.42
-2.00	-2.00	-1.62	0.38	0.34	0.39
0.00	0.00	0.36	0.36	0.29	0.30
2.00	1.80	2.33	0.53	0.29	0.33
4.00	3.85	4.25	0.40	0.28	0.29
6.00	5.90	6.40	0.50	0.29	0.36
8.00	7.95	8.61	0.67	0.27	0.37
10.00	9.89	10.64	0.75	0.30	0.36
12.00	11.95	12.55	0.60	0.27	0.35

Note that the RMS values of the 5-hole probe-transducer system are larger than those of the β vane-pot system. This suggests that in terms of precision, the β vane-pot system has better performance. In an effort to explore the possibility of a scaling relationship between the β values from the β vane-pot and 5-hole probe-transducer system, the mean values were plotted against each other as shown in Figure V.14. A curve fitted equation of β(from β vane) = 0.9692 x β(from 5-hole probe) - 0.3456 was obtained and is not unreasonably far from the ideal equation of β(from β vane) = 1.0 x β(from 5-hole probe).

y = 0.9692x - 0.3456
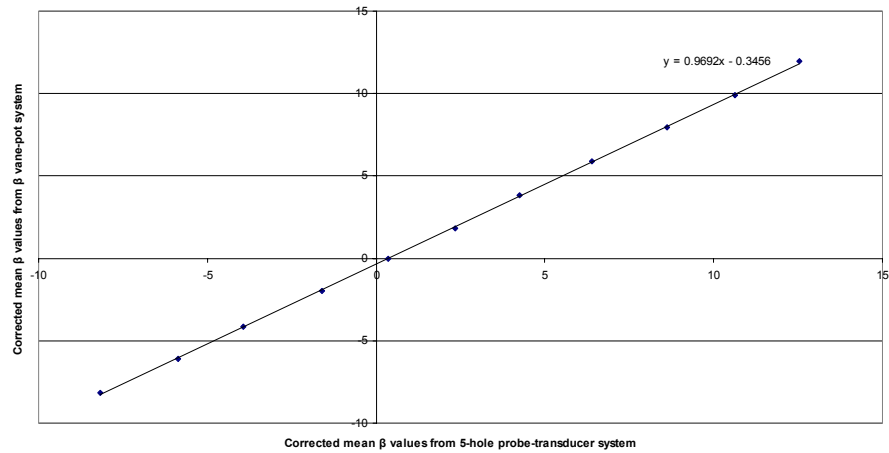
Figure V.14 Relationship of β values from β vane-pot and
5-hole probe-transducer system

The scaling relationship was applied to the β signal
in Figure V.12. Figure V.14 shows the results. Note that
both signals were in very close agreement after the scaling
was applied to the signal from the 5-hole probe-transducer
system.
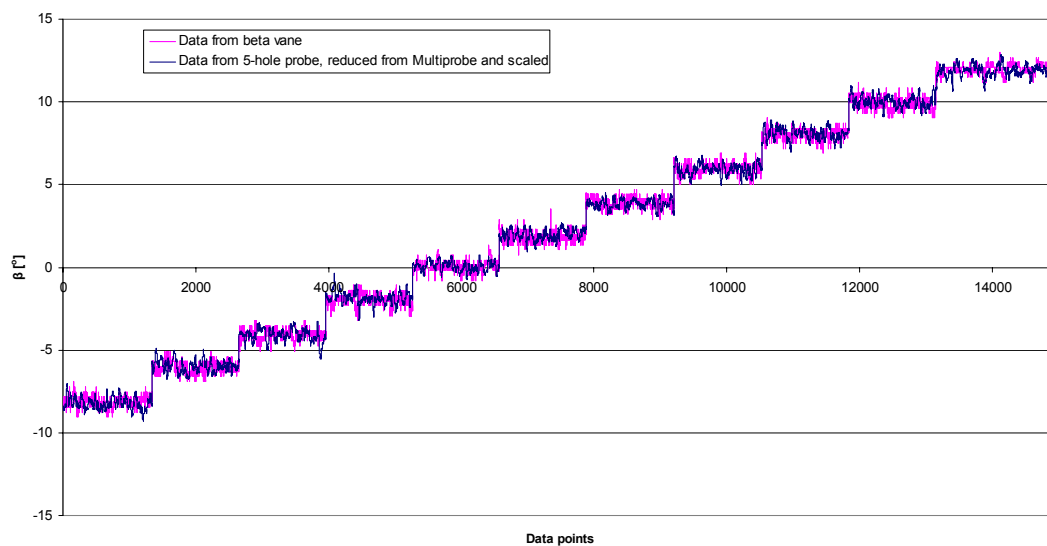
Figure V.15 Scaled data from 5-hole probe

71

A PSD analysis was conducted and the PSD plots are as shown in Figure V.16. For comparison purposes, the PSD of the test-flight β signal from the β vane-pot system on the FROG was superimposed (green curve in Figure V.16). Note the significant larger power of the test-flight β signal as compared to those from the β vane-pot and 5-hole probe-transducers in the wind tunnel experiment. This can be accounted by the fact that aircraft vibrations and other flight operating environment effects were present during the test flight (which is not present in the wind tunnel experiment). Figure V.16 also shows that both the 5-hole probe-transducer system and β vane-pot system have approximately the same bandwidth. The β vane-pot system has better roll-off performance than the 5-hole probe-transducer system. In terms of out-of-band frequencies (approximately above 2 hertz), the 5-hole probe-transducer has better attenuation than the β vane-pot system.
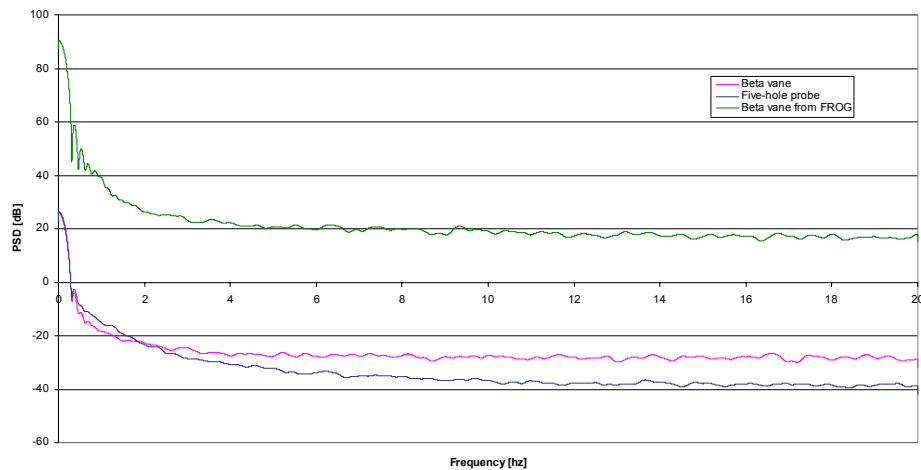
Figure V.16 PSD plots of β signal from 5-hole probe and β pot (wind tunnel and on the FROG)

72

Figure V.17 shows the result of the second part of the experiment which was dynamically measuring β by sweeping from -10° to 12° and back to -10°. Note that the sweep of β from -10° to 12° occurred at a different sweep rate from the sweep of β from 12° back to -10° as the turntable mount of the wind tunnel has a sweep rate of 4.5° per second when β is increasing and 5° per second when β is decreasing.
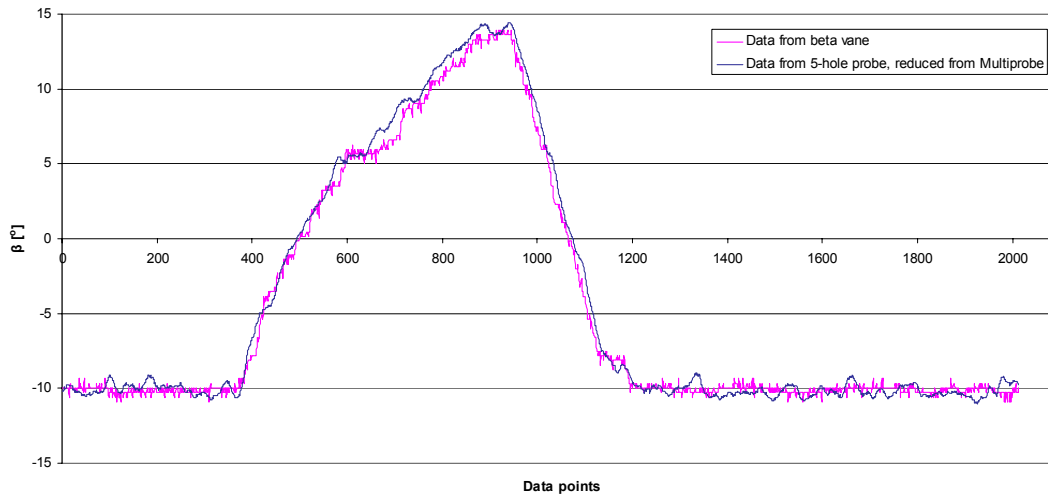
Figure V.17 Dynamic measurement of β from 5-hole probe and β pot

Upon careful scrutiny of Figure V.17, as β was swept increasing from -10° to 12° at a rate of 4.5° per second, the signal from the 5-hole probe-transducer system was leading the signal from the β vane-pot system for most of the time; this can be observed from the 400th to the 950th data point. When β was swept decreasing from 12° back to -10° at a rate of 5° per second, the signal from the β vane-pot system was instead leading the signal from the 5-hole

probe-transducer system; note the 950th to the 1200th data point. A hysteresis effect is observed here. In this dynamic case, a parameter of interest for the 5-hole probe-transducer system will be the lag constant which, in [1] is given as

$$\lambda = \frac{128\mu LV}{\pi d^4 P} \tag{12}$$

Where:

μ is the coefficient of viscosity of air

L is the total length of tubing used

V is the combined volume in tubing and transducer cavity

D is the internal diameter of the tubing used

P is the reference pressure in the tubing

Since a total length of approximately 6 feet of tubing (internal diameter 1/32 inch was used), the lag constant for the 5-hole probe-transducer was determined to be 0.12 seconds. For applications of pressure measurements, it is reasonable to assume that the lag constant of 0.12 seconds is not an issue.

5.   Use of 5-Hole Probe on the FROG

The pressure configuration on the 5-hole probe used in the wind tunnel experiment was that each of the port

pressures was referenced to the atmospheric pressure. For the FROG, a few configurations are possible. The first configuration is such that five absolute pressure transducers are used for measuring the port pressures. Another possible configuration will be using transducer B type (differential type) and referencing each of the port pressures to the static pressure of the FROG; however, an absolute pressure value of the static pressure is required (which implies the use of five differential transducers and one absolute transducer) by Multiprobe© for data reduction.

The last possible configuration is using only four transducer B type and referencing all the port pressures to the center port pressure. This configuration allows Multiprobe© to compute $\alpha - \beta$ from only the u-v-w component of velocity. But the total pressure and static pressure values reduced from Multiprobe© cannot be used as the reference pressure in this case will be unknown. But since the subject of interest is really only $\alpha - \beta$, this configuration is recommended for use on the FROG as it minimized the number of transducers used, allows simpler pressure tubings installation and reduces the number of channels for data acquisition.

THIS PAGE INTENTIONALLY LEFT BLANK

VI DISCUSSION

A.   SENSOR CALIBRATION

The calibration of the pressure transducer and the α-β pots is of great importance, as a good calibration will give accurate air data that is desired. A good engineering practice is that the sensors are to be calibrated in the laboratory (just the sensors with the same processor acquiring data in flight) and on the aircraft before and after test flights. The three calibration results are then evaluated, compared and modified as necessary. As far as this thesis is concerned, the sensors were calibrated in the laboratory and on the FROG before the test flight. The calibration results were in close agreement. However, as the FROG was lost due to an air accident during the test flight on 9 Oct 2001, the calibration after the test flight could not be carried out. Nevertheless, the initial two calibrations carried out were deemed to be sufficient.

As far as the calibration of the 5-hole probe is concerned, it is not an issue as it is done by the manufacturer. The calibration for the 5-hole probe is a highly-accurate, more than two thousand point calibration. It also includes a post calibration error analysis and quality control. Since the FROG is operating at the low Mach number range, calibration at a single speed is sufficient for the 5-hole probe.

B.   RESOLUTION

Since the air data signal had been digitized, one issue that arises is the resolution or quantization level of the digitized signal. The digitized signal is an integer number of counts basically. The resolution of a signal is exactly one count which corresponds to an engineering unit that depends on the sensor calibration. In the case of the FROG, the engineering units of interest are meters per seconds (airspeed) and degrees ($\alpha - \beta$). As mentioned in Chapter II, the resolution of the pressure transducer is approximately 0.008 meters per second and 0.09° for the $\alpha - \beta$ pots. It was concluded from [6] that as long as the resolution magnitude is much smaller than the noise level of the digitized data, it is very much acceptable since it allows detection of small variations of the analog input signal.

The data used for plotting Figures III.5 through III.10 which presented the air data signal before and after filtering, was used to determine the average nose level. The average noise level for the pressure transducer (transducer A) was found to be 26 digital counts which translate to a 1.25 meters per second noise level. The average noise level of for the $\alpha - \beta$ pots was found to be 0.1°. It is obvious that the resolution magnitude of the pressure transducer is significantly lesser than its noise level. Therefore, as far as the resolution level for the pressure transducer, it is much acceptable based on the processor with a 12-bit analog to digital converter. But

the α-β pots do require an analog to digital converter that is more than 12-bit.

C.   REAL-TIME PROCESSING OF AIR DATA

The air data in this project was post-processed rather than real-time processed. The fact that air data was post-processed presented a great degree of simplicity for this project as far as processing of air data is concerned. If real-time processing of air data is desired, MATLAB® Real Time Workshop can be used. The research effort in real-time processing of air data is currently being pursued in [9]. In Real Time Workshop, filtering, re-sampling, calibration and corrections sub-modules have to be created in order for it to perform real-time processing. In particular, the calibration, static and dynamic correction results from this thesis have to be implemented and created as a sub-module in Real Time Workshop. Filtering and re-sampling also have to be built in as a sub-module into Real Time Workshop. Real-time processing of air data also can be integrated together with the wind estimation model as mentioned in Chapter III Section F to provide real time wind estimation which is crucial for Chem/Bio attack response. Real-time processing of air data with proper display provides the pilot of the FROG with a form of real time feedback which is also beneficial.

D.   PRESSURE TRANSDUCER A VERSUS PRESSURE TRANSDUCER B

Chapter V covered in detail the experiment conducted to compare both transducers A and B. Both transducers exhibit the same bandwidth and roll-off. But in terms of

out-of-band frequencies, transducer B does suggest that is has better attenuation. However, to be complete, issues pertaining to other transducers characteristics like age, linearity, repeatability and environmental effects have to be also thoroughly researched. In terms of frequency response and noise characteristics, the wind tunnel experiment results as presented in Chapter V do suggest that transducer B is a more favorable choice for future use in the FROG.

E. $\alpha - \beta$ VANE-POT SYSTEM VERSUS 5-HOLE PROBE-TRANSDUCER SYSTEM

The details of the results from the wind tunnel experiment conducted to compare both $\alpha - \beta$ vane-pot and 5-hole probe-transducer systems were covered in Chapter V. As mentioned before, the RMS value of the signal achieved by the 5-hole probe-transducer system is larger than that of the β vane-pot system. Since a lower RMS value is desired, this indicated that the β vane-pot system is better in this aspect. For frequency response, both the 5-hole probe-transducer system and β vane-pot system has approximately the same bandwidth. The β vane-pot system has better roll-off performance than the 5-hole probe-transducer system and in terms of out-of-band frequencies; the 5-hole probe-transducer has better attenuation than the β vane-pot system.

Both the measurement systems have to be subjected to a real flight operating environment and be tested in flight. This will provide a more comprehensive review and

comparison of both measurement systems as the experiment in the wind tunnel alone is not sufficient to simulate the real flight operating environment, for example, the noise level in wind tunnel and in flight definitely differs a significant amount for the α-β vane-pots system. However, the wind tunnel experiment did reveal an important fact: the 5-hole probe-transducer is capable of measuring α-β on the FROG.

THIS PAGE INTENTIONALLY LEFT BLANK

VII CONCLUSIONS AND RECOMMENDATIONS

A.   CONCLUSION

The air data system using standard sensors was installed on the FROG after consideration of air data error associated with several locations of the sensors on the FROG. A test flight was carried out and air data was acquired successfully. The post processing of the air data which include filtering, re-sampling, calibrating, static and dynamic correction (numerical simulation for static source correction) were carried out as well. Preliminary wind extraction was carried out (refer to [9]) from the post processed air data and results are very promising as the preliminary wind estimation was found to be in close agreement with wind data from the Meteorology Department. Further wind extraction will be carried out and researched in [9].

Pressure transducers were compared by running wind tunnel experiments and analyzing the quality of output signals from the transducers.

A 5-hole probe-transducer system was also used in a wind tunnel experiment to compare with the $\alpha - \beta$ vane-pot system. The performance of the 5-hole probe-transducer and the $\alpha - \beta$ vane-pot system were analyzed and discussed in terms of RMS values and frequency response.

Specific issues pertaining to air data acquisition were also explored and discussed. This thesis project will pave the way for the UAV to be used for Chem/Bio attack

response. Use of a UAV to make in situ measurements of particulates as well as air and inertial data for winds extraction is a unique contribution to the area of homeland security.

B.   RECOMMENDATIONS

With the success completion of this thesis effort, the following can be pursued in the near future:

1.   The change-out and addition of specific components within the air data system; a 16-bit or higher analog to digital converter in the processor can be used instead of the current 12-bit analog to digital converter. Since pressure transducer B has better frequency response and is less noisy than transducer A, it is also recommended that pressure transducer B be used for the pitot static pressure measurement and/or 5-hole probe pressure measurement. Since the density correction of the air data was carried out with data from the Meteorology Department (as mentioned in Chapter III), it is also recommended that the FROG be installed with pressure altitude and temperature sensors so that the exact density of the FROG at a particular altitude can be computed. This allows a more accurate density correction to be carried out.

2.   Use of more advanced numerical software for the dynamic correction; PSW$^{\copyright}$ was used to make off-body flow analysis to calculate the corrections to be made to the air data. The software suite had since been updated to a newer windows version. Therefore, it is recommended that the newer version or more advanced numerical software be used.

The challenge for more advanced numerical software however will be to re-create the numerical model (grid) of the FROG in the new software.

3.   Using Real Time Workshop in MATLAB®, establish a real-time air data processing system instead of the current way of post processing air data. It is also recommended that Multiprobe© be integrated into Real Time Workshop in MATLAB® to allow real-time data reduction from the pressure readings obtained from the 5-hole probe. This requires consultation with the manufacturer of the 5-hole probe.

4.   Test flight both the β vane-pot and 5-hole probe-transducer on the FROG to compare the performance of both $\alpha - \beta$ measurement systems. Together with the findings from the wind tunnel experiment conducted in this project, a decision can be then made to select the appropriate $\alpha - \beta$ measurement system.

THIS PAGE INTENTIONALLY LEFT BLANK

APPENDIX A. DESCRIPTION OF FOG-R UAV EXTRACTED FROM [10]

Tactically Expendable Remote Navigator (TERN)

TERN is an acronym for "Tactically Expendable Remote Navigator. This versatile UAV is capable of a variety of missions, recoverable in peacetime training missions, yet of sufficiently low cost to be discarded after actual battle if necessary. A variant of the vehicle, FOG-R, has been flown non-line-of-sight (NLOS) "over and beyond the hill," using a Fiber Optic Data Link (FODL) for command uplink and video downlink. This FOG-R version is jam-proof. Another variant, TERN-C, has carried a remote sensor for detecting chemical warfare agents.

The TERN is designed to carry up to 22 lbs. (10 kg) of payload for periods of up to four hours. The wing is fitted with flaps which can be trimmed to provide slow flight speed for surveillance and extended to facilitate tight landings.

TERN's optional equipment includes a programmable autopilot, GPS navigation, video system, and other electronic sensors.

THIS PAGE INTENTIONALLY LEFT BLANK

APPENDIX B. DETAILED SPECIFICATIONS OF SENSOR EXTRACTED FROM [11]

VISHAY

Model 140, 142
Vishay Spectrol

1/2" (12.7mm) Single - Turn Wirewound Precision Potentiometer

Model 140 Bushing Mount

Model 142 Servo Mount

FEATURES
- 50Ω to 20KΩ
- Bushing or Servo

ELECTRICAL SPECIFICATIONS

PARAMETER	STANDARD	
Total Resistance	50Ω to 20KΩ	
Tolerance	± 5%	
Absolute Minimum Resistance	Linearity x Total Resistance or 0.5Ω, whichever is greater	
Linearity (Independent)	± 1.0%	
Noise	100Ω ENR	
Power Rating	2 watts at 40°C ambient derating linearly to zero at 125°C	
Insulation Resistance	1,000MΩ min. 0.500VDC	
Dielectric Strength	1.000V$_{RMS}$, 60 Hz	
Rotation	140 320° ± 5°	142 350° + 0° - 4°
End Voltage	Linearity x total applied voltage for total resistance above 20Ω; 2.0% of total applied voltage for 20Ω and below	

MATERIAL SPECIFICATIONS

Shaft	Stainless steel, non magnetic non-passivated
Housing	Aluminum, anodized
Rear Lid	Molded glass filled thermoset plastic
Terminals	Brass, gold plated
Mounting Hardware Lockwasher Internal Tooth: Panel nut:	(Model 140 only) Steel, nickel plated. Brass, nickel plated

ENVIRONMENTAL SPECIFICATIONS

Vibration	20G thru 2000 Hz
Shock	50g
Salt Spray	96 Hours
Rotational Life	500,000 Shaft Revolutions
Load Life	900 Hours
Temperature Range	- 55°C to + 125°C (operating)

ORDERING INFORMATION

This part number consists of four groups of digits. The first group is the Spectrol model number. The second digit describes the mechanical options available. The third digit describes the other optional features which can be supplied. The fourth group is the standard EIA resistance code.
Example: 140 - 0 - 0 - 203

140	0	0	203
MODEL	MECHANICAL OPTIONS	OTHER OPTIONAL	RESISTANCE CODE FEATURES
Bushing 140	0. Stops, Slotted Shaft (std) 1. Plain Shaft 2. Shaft Lock 3. Continuous Rotation 4. Combination 1 & 2 5. Combination 1 & 3 6. Combination 2 & 3 7. Combination 1, 2, & 3	0. Standard Torque 1. Center Tap (10K max. Rt) 2. High Torque 3. Sealed Construction 4. Combination 1 & 2 5. Combination 1 & 3 6. Combination 2 & 3 7. Combination 1, 2, & 3	2 = First Significant figure 0 = Second significant figure 3 = Number of zeros following
Servo 142	0. Continuous Rotation, Plain Shaft (std.)	0. Standard Torque 1. Center Tap (10K max. Rt)	Same as above

Example: Part number 140-0-0-203 describes bushing mount 140 with stops, slotted shaft, standard torque and resistance of 20KΩ

89

Model 140, 142

VISHAY

Vishay Spectrol   1/2" (12.7mm) Single - Turn Wirewound
Precision Potentiometer

DIMENSIONS in inches (millimeters)

BUSHING MOUNT

SERVO MOUNT

TOLERANCES: UNLESS
OTHERWISE NOTED,
DECIMALS ± 0.005, ANGLES ± 2°

CENTER TAP AVAILABLE AS
SPEC STANDARD FEATURE
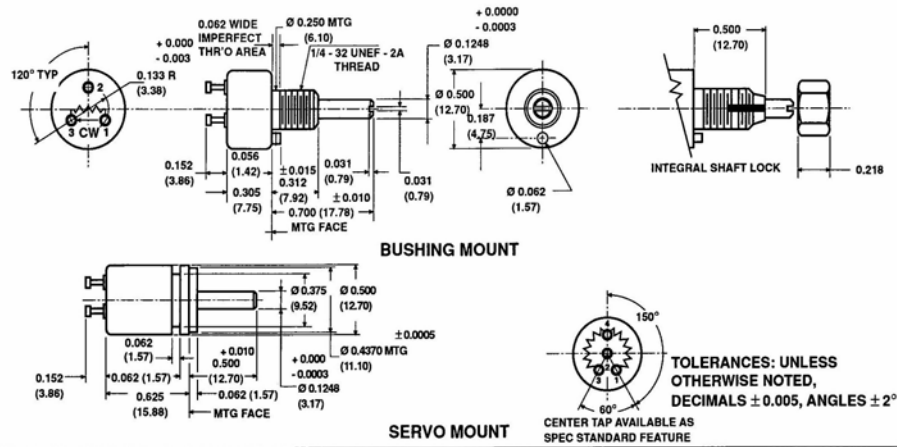
MECHANICAL SPECIFICATIONS

PARAMETER		
Rotation	140 330° ± 5°	142 360° continuous
Bearing Type	SLEEVE BEARING	BALL BEARING
Torque (Maximums)		
Starting	0.2 oz - in (14.40gm - cm)	0.075 oz - in (5.40gm - cm)
Running	0.2 oz - in (14.40gm - cm)	0.05 oz - in (3.60gm - cm)
Traversing	–	–
Dead Zone	Not applicable	0.20 oz - in (14.40gm - cm)
Weight	0.1 oz. maximum (2.84gm)	0.3 oz (8.50gm) maximum
Stop Strength	5 in - lbs (5.76 kgm - cm) static (140 only)	
Runouts (Maximum)	140	142
Shaft (TIR)	0.002 in (0.05cm)	0.002 in (0.05cm)
Pilot Dia (TIR)	0.002 in (0.05cm)	0.002 in (0.05cm)
Lateral (TIR)	0.003 in (0.08cm)	0.002 in (0.05cm)
Shaft End Play	0.006 in (0.15cm)	0.004 in (0.10cm)
Shaft Radial Play	0.003 in (0.08cm)	0.002 in (0.05cm)

POWER RATING CHART
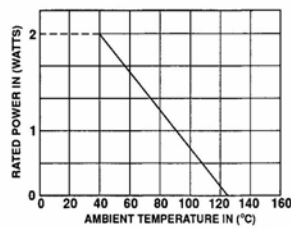
MARKING

Unit Identification	Units shall be marked with manufacturer's name, model number, resistance value & tolerance, circuit diagram, terminal identification, linearity & date code

RESISTANCE ELEMENT DATA

STD RESISTANCE VALUES (Ω)	RESO- LUTION (%)	OHMS PER TURN	MAXIMUM CURRENT AT 40°C AMBIENT (mA)	MAXIMUM VOLTAGE ACROSS COIL (V)	WIRE TEMP. COEF. (ppm/°C)
50	0.542	0.271	200.0	10.0	20
100	0.431	0.431	141.0	14.1	20
200	0.361	0.722	100.0	20.0	20
500	0.312	1.56	63.2	31.6	20
1K	0.255	2.55	44.7	44.7	20
2K	0.197	3.94	31.6	63.2	20
5K	0.170	8.50	20.0	100.0	20
10K	0.147	14.7	14.1	141.0	20
20K	0.105	21.0	10.0	200.0	20

APPENDIX C. OVERVIEW OF PERSONAL SIMULATION WORKS EXTRACTED FROM [4] (LOFTSMAN, CMARC AND POSTMARC)

A.   GENERAL

Personal Simulation Works is a PC based software suite that provides for the three primary CFD requirements; 3D modeling of an aircraft (LOFTSMAN), panel code flow solver (CMARC), and post-processing of the computed flow field (POSTMARC). The software package contains three applications hosted on the IBM compatible personal computer. Each software program is discussed separately.

B.   LOFTSMAN

LOFTSMAN is a Windows hosted ad modeling tool that generates surface panel distributions for CMARC or PMARC input files. The program is based on conics, which allows rapid lofting of streamlined bodies such as aircraft fuselages and engine nacelles. In addition, wing and control surfaces can be desired with the extensive library of airfoil templates or with user specified coordinates. The software is well decremented, including a tutorial, in the Personal Simulation Works User Guide. LOFTSMAN is primarily designed for creating new objects, but an existing airframe can be matched quite closely with just a detailed three-view drawing that includes frame cross sections.

1.   Streamlined Bodies

LOFTSMAN functionality is divided into Body Objects and Wing Objects. In general, they remain separate unless the intersection between a wing and body is required. Body Objects are created using a family of curves called second-degree conics. Circles, ellipses, parabolas and hyperbolas are among this group. An entire fuselage is described by specifying just four lines. These are the top waterline (TW), bottom waterline (BW), the maximum breadth line (MB) and the waterline of the maximum breadth line (WW). For each line, the beginning, ending and a few points along the line are specified. Control points are also specified with a curvature factor that allows LOFTSMAN to generate a smooth conic between the points.

2.   Wings and Control Surfaces

Wings and control surfaces are easily specified in LOFTSMAN using a short input file created with any text editor. The file specifies root, intermediate and tip rib section, location, axis, chord and incidence. LOFTSMAN then fairs a smooth surface through the rib sections. Washout is specified by varying the incidence of the root and tip ribs. Sweep-back is controlled by staggering the tip rib location with respect to the root ribs. Once the general wing surface is specified, control surfaces such as ailerons, flaps and elevators can be deflected and meshed.

92

3.   Patches

LOFTSMAN automatically meshes 3D surfaces and creates patches for CMARC/PMARC input files. The distinction between a mesh and a patch is important. A mesh is a set of quadrilateral and triangular panels that represent the surface of a wing or body. When the set of panels is organized and formatted to create a sub-component portion of a CMARC or PMARC input file, it is called a patch.

A body or wing surface is first meshed at a density specified by the user. Panel compression options include cosine and half-cosine spacing. After meshing the object, one saves it to a text file as a formatted patch. One then opens the patch file with any text editor and copies/pastes the patch text into the appropriate location in the CMARC input file.

Each control surface deflection requires a separate mesh and formatted patch. For instance, to evaluate roll performance one needs to separately mesh an upward aileron deflection on the right wing and a downward deflection on the left wing. If multiple deflections of a single control surface are required, each deflection must be meshed separately.

C.   CMARC

CMARC is the C version of PMARC low-order panel code. Inviscid, irrotational, incompressible, potential flow is assumed. Low-order means that source and doublet strength distribution is constant across a panel. There is no

attempt to match that source or doublet strength of an adjacent panel at a common edge. Advanced features include internal flow modeling and time stepping wake models.

PMARC version 12.19 was released as FORTRAN 77 source code in 1992. CMARC was rewritten in the C language and compiled for hosting on IBM compatible personal computers by Aerologic, Inc. The program runs under the DOS operating system. It will also run in a DOS window from Windows 3.1, 95, 98, 2000 or XP. Enhanced features include command-line options and flexible memory management. Command line options simplify batch processing by adding an extensive set of switches that can be set external to the CMARC input ale. Flexible memory management provides for the automatic sizing of arrays without having to recompile the source code.

D.   POSTMARC

POSTMARC is a Windows post-processing program for the visualization of CMARC and PMARC output files. Capabilities include body geometry, wake stepping, surface pressure and streamline visualization. POSTMARC also provides the capability to integrate pressure and skin action forces over the model geometry. This proves particularly useful when one desires to recalculate loads around a different center of gravity.

An interesting feature for design work is the integration of panel surface area to total wetted area. After lofting a new geometry in LOFTSMAN, a quick check of geometry is made by running CMARC with the in command line

toggle. The total wetted area is then checked in POSTMARC. This function is particularly useful when working to reduce skin friction drag.

Versions 1.17.3 and later of POSTMARC include the capability to integrate skin friction drag coefficient over the model geometry. It is important to note that a key piece of the drag equation is missing from a POSTMARC solution. CMARC provides induced drag from the surface pressure distribution and skin friction drag from the 2D boundary layer code. Skin friction is only calculated up to the point of boundary layer separation. Pressure drag due to separation, a major portion of the drag equation, is missing from a CMARC/POSTMARC solution.

THIS PAGE INTENTIONALLY LEFT BLANK

APPENDIX D. DETAILED SPECIFICATIONS OF PRESSURE TRANSDUCER B EXTRACTED FROM [12]

SERIES 850 BOARD–MOUNTABLE PRESSURE TRANSDUCER

ISO 9001 CERTIFIED
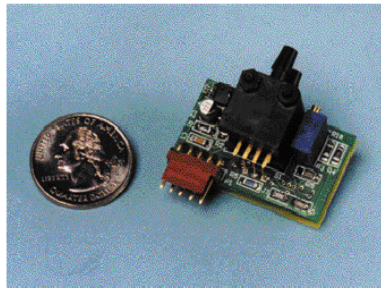
Specifications

Accuracy:*	+/- 1% F.S.O.
Stability:	+/- 0.5% F.S.O./yr.
Thermal Effects:(zero)	+/-0.075% F.S.O./°C
	(+/-0.042%F.S.O./°F)
0.5" Range	+/-0.150% F.S.O./°C
	(+/-0.083%F.S.O./°F)
Thermal Effects:(span)	+/-0.005% F.S.O./°C
	(+/-0.003%F.S.O./°F)
Overpressure:	20 PSI or 2x FSP whichever is greater
Pressure Range:	0.5" WC to 40 PSI (Custom & Bi-directional ranges available)
Compensated Range:	10° to 50°C (50° to 122°F)
Media:	Limited only to media that will not attack Polyphenylene Sulfide (PPS), Polyetherimide (PEI), Silicon, or Fluorosilicone, Silicone RTV. Note that liquids are allowed in either or both ports.
Operating Humidity:	90% RH non-condensing
Operating Temp:	-25°C to 70°C (-13 to 158°F)
Input Supply:	12-24 VDC
Supply Current:	< 10mA
Load Resistance:	2KΩ minimum
Output Signal:	1-5 VDC, 1-6VDC, 1-10VDC** (call for custom voltage outputs, most available)
Adjustments:	Offset 60% of F.S.O. minimum
Electrical Connections:	0.025" square pins on 0.1" centers (5)–Board Mountable***
Pressure Connections:	Barbed fitting for 1/8" I.D. tubing
Dimensions:	Approx. 1.50" x 1.35" x 0.9" (3.81cm x 3.43cm x 2.29cm)

*   Includes non-linearity, hysteresis, and non-repeatability at a fixed temperature

**   18-24VDC input required for 1-10VDC output

***   Direct-to-board solder connection version available upon request, also optional cable available

Features & Applications

- Excellent long–term stability!

- Fully compensated and signal conditioned!

- Optional cable available for low–cost stand alone applications.

- Great for applications such as fume hoods, clean rooms, VAV, duct static, medical applications and many more!

- Can be used on some water applications!

- Virtually no position sensitivity!

- Custom ranges available!

- Standard 2–year warranty!

- Direct to board solder connection available for easy integration into most OEM products.

For the Most Recent Product Information Visit Our Website at www.autotraninc.com

AutoTran
INCORPORATED

7424 Washington Avenue South • Eden Prairie, MN 55344
(800) 735-8998 • (952) 942-8743 • FAX (952) 942-8753
www.autotraninc.com

ID Number 1210-137   Page 1 of 2   Revision C   Issue Date: 2/26/02

Note:
1. P1 pins on .1" centers

2. Mount to substrate (PCB) using hardware shown above.

3. Use cable from P1 to connect to other circuity

Not Shown: Direct-to-Board solder connection version. Consult factory for drawing.
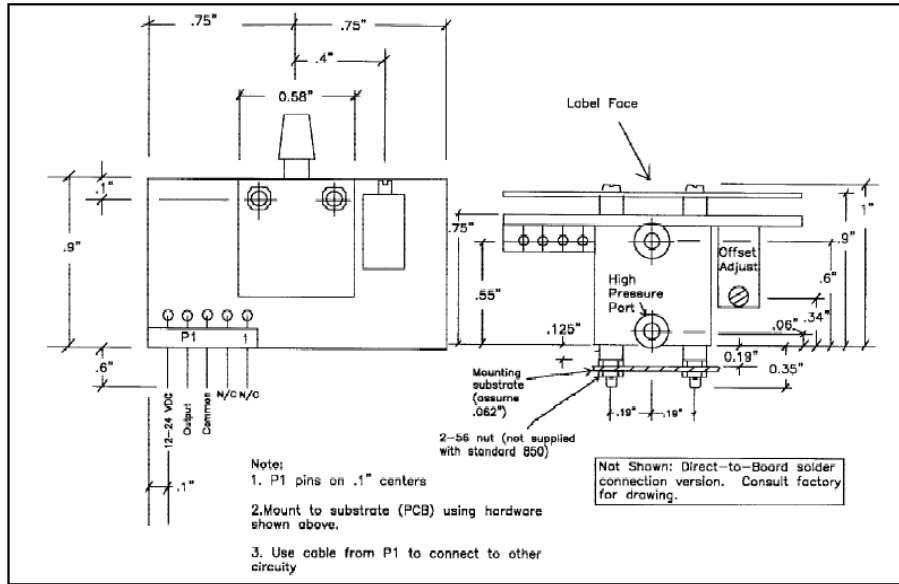
How to Order

A typical order number consists of the model number, type, pressure range, input supply, and output signal.

Model	Type	Pressure Range	Input Supply	Output Signal
850	D = Differential	User desired range	12D = 12-24 VDC	0 = 1-5 VDC
	or Gage*	from 0/0.5" WC - 0/40 PSI	24D = 18-24 VDC	1 = 1-6 VDC
		(Bi-directional ranges available)		2 = 1-10 VDC**
				5 = custom output

Example: 850D 5" WC 12D4 (Model number 850, differential or gage type unit, pressure range of 0-5" WC, input supply of 12-24 VDC, output signal of 1-5VDC)

* With a gage application, one of the two pressure ports is vented to atmosphere.
** Requires 18-24 VDC input

Optional Items
ABS plastic enclosure

Warranty

Any regular Auto Tran product that proves to be defective in material or workmanship within a warranty period of two (2) years will be repaired or replaced when returned freight prepaid.

Note: Auto Tran reserves the right to change its specifications at any time, without notice. Auto Tran is not expert in the customer's technical field and therefore does not warrant the suitability of its product for the application selected by the customer.

LIST OF REFERENCES

[1] Gracey, William, *Measurement of Aircraft Speed and Altitude*, pp 1-262, John Wiley and Sons, June 1981.

[2] National Aeronautics and Space Administration Langley Aeronautical Laboratory, NACA TN4351, *Summary of Methods of Measuring Angle of Attack on Aircraft,* Gracey, William, Aug 1958.

[3] National Aeronautics and Space Administration Dryden Flight Research Center, NASA Technical Memorandum 104316, *Air data Measurement and Calibration,* Haering, Jr Edward, 1995.

[4] Pollard, Stephen. *Development and Verification of an Aerodynamic Model for the NPS FROG UAV using the CMARC Panel Code Software Suite,* Master's Thesis, Naval Postgraduate School, Monterey, California, 1998.

[5] *Performance Phase Textbook,* v.1., USAF Test Pilot School, Edwards AFB, June 1988.

[6] Maine, R.E. and Iliff K.W., *AGARD Flight Test Techniques Series,* v.3, AGARD, 1986.

[7] Aeroprobe Corporation, *Multi Hole Probe Information Packet,* 1.5[th] Ed, October 2001.

[8] Schmidt, Louis, *Introduction to Aircraft Flight Dynamics*, AIAA Education Series, 1998.

[9] Sir, Cristian, *Real Time Wind Estimation for Chem/Bio attack Response*, Master's Thesis, Naval Postgraduate School, Monterey, California, 2003 (To be published in Jun 2003).

[10] BAI Aerosystems Inc, *Tactically Expendable Remote Navigator,* [http://www.baiaerosystems.com/tern.html], Mar 2003.

[11] Vishay Inc, *Model 140, 142 Potentiometers* [http://www.vishay.com/docs/57039/140142.pdf], Mar 2003.

[12] AutoTran Inc, *Series 850 Transducer,* [http://www.autotraninc.com/850.html], Mar 2003.

INITIAL DISTRIBUTION LIST

1. Defense Technical Information Center
   Ft. Belvoir, VA

2. Dudley Knox Library
   Naval Postgraduate School
   Monterey, CA

3. Assoc Prof. Richard M Howard
   Dept. of Aeronautics and Astronautics
   Naval Postgraduate School
   Monterey, CA

4. Dr. Vladimir Dobrokhodov
   Dept. of Aeronautics and Astronautics
   Naval Postgraduate School
   Monterey, CA

5. Assoc Prof. Isaac I Kaminer
   Dept. of Aeronautics and Astronautics
   Naval Postgraduate School
   Monterey, CA

6. Prof. Max Platzer
   Dept. of Aeronautics and Astronautics
   Naval Postgraduate School
   Monterey, CA

7. Capt Tan, Kwang Liang
   Republic of Singapore Air Force
   Ministry of Defense Singapore
   Singapore